



*Escuela Técnica Superior de
Ingenieros de Caminos, Canales
y Puertos.*
UNIVERSIDAD DE CANTABRIA



A Two-Way Coupled Eulerian One-Fluid Numerical Method for Fluid-Sediment Interaction.

Trabajo realizado por:
Julio García-Maribona López-Sela

Dirigido:
Javier López Lara
Íñigo Losada Rodríguez

Titulación:
**Máster Universitario
en Ingeniería Costera
y Portuaria**

Santander, Octubre de 2018

TRABAJO FINAL DE MASTER



Contents

1. Introduction.	1
2. State of the art.	4
2.1. Eulerian One-fluid models description.....	5
2.1.1. Hydrodynamic model.	5
2.1.2. Sediment transport model.	8
2.1.2. Morphology model.....	14
2.1.3. Coupling hydrodynamics and morphology models.....	17
2.1.4. Summary.	18
3. Implementation.....	20
3.1. Hydrodynamic model.	20
3.2. Bedload module.	21
3.2.1. Friction velocity.	22
3.2.2. Landslide mechanism.	22
3.2.3. Determining the velocity of particles.	22
3.3. Suspended transport module.....	23
3.3.1. Solving advective-diffusive transport equation.	23
3.3.2. Interpolation of magnitudes.	25
3.3.3. Boundary conditions.	28
3.4. Sediment balance module.....	30
3.5. Moving bed module.	31
4. Model test.	34
4.1. Test case 1: sedimentation.	34
4.2. Test case 2: sediment diffusion.....	37
4.3. Test case 3: landslide mechanism.	39
5. Validation.	42
6. Conclusions.	49
7. Further work.....	50
References.....	53



1. Introduction.

Problems related with sediment transport and scour processes have been acquiring importance in marine and coastal engineering as structures are exposed increasingly adverse hydrodynamic conditions.

Some examples of problems where sediment transport is involved are:

- Scour close to breakwaters: can be generated by different processes such as standing waves, breaking waves or overtopping discharges. The case of standing waves can be important if the resulting scour pattern is able to change the incoming wave conditions, in particular, the worst scenario is a vertical breakwater originally designed for pulsating waves in which the scour pattern produces wave breaking at the wall, leading to impulsive forces. Scour generated by overtopping discharges can compromise the stability of the breakwater, this could occur during a tsunami event or strong storm for instance. The toe of breakwaters is another problematic place where scour can develop and lead to failure of the structure.



Figure 1: Scour in front of rubble mound breakwaters.. Image from (Papadopoulos, 2013).

- Scour around foundation of monopiles or other offshore structures: This can be the case of foundations for offshore wind turbines, oil rigs or other kind of facilities. The vortical structures generated around a cylinder in waves, currents or combination of both produce a local scour that can reach the order of magnitude of the cylinder's diameter. When this scour affects the foundation, it removes material that is contributing to its stability. In groups of cylinders, the resulting scour is a combination of local scour around each of them and a global scour around the whole structure, this combination can lead to even larger scour than for an isolated cylinder. The same situation occurs in bridge piles on rivers during flood events and it is a critical point in the design of the whole structure, and it is precisely in flood conditions when these infrastructures are more needed for emergency teams or evacuations.



Figure 2: Railway bridge collapse in Ireland caused by scour undermining in piers. Image from <https://www.newcivilengineer.com/scour-revealed-as-cause-of-irish-bridge-collapse/5207460.article>

- Scour in submarine pipes and self-burial: Submarine pipes can be designed to be buried or laying on the seabed. In both cases, if the scour produced by waves or currents is large enough, scour can appear beneath them. This generates a span under the pipe that changes its structural behavior leading to high bending moments. In some cases when the pipe bends a self-burial process develops. Submarine pipes and conductions can provide connections for electrical interchange or optic fiber communications between countries or connection between offshore energy production facilities and inland consume points.
- Scour in mooring facilities induced by propeller wakes: the continuous increase in ship sizes and the corresponding increment in propulsion power is generating this kind of problems in ports with high affluence of cruises and fast ferries. The scour generated at the basement of mooring structures can lead to structure displacements incompatible with the service or even compromise its stability. This topic is addressed in various design recommendations for port facilities such as PIANC report and R.O.M., as it is becoming a crucial element for port adaptation to new demands from maritime traffic.

Design of protections for against scour is therefore fundamental. However, this task must be done carefully, as they often require a great amount of material and its cost can be elevated. In addition, the failure of these protections can eventually lead to the collapse of the whole structure as explained before. Various techniques are available to handle scour issues such as protective covers made of rockfill, concrete blocks or geotextiles.

There are three different options that can be used to evaluate sediment transport problems and design solutions if needed: semi-empirical formulae, physical modelling and numerical modelling. The decision of which one should be used depends on the complexity of the problem, although a combination of them is usually the most efficient and safe approach.

There exist different semi-empirical formulae for common configurations such as sediment transport in waves, currents or scour around cylinders. Sometimes there is no specific formulae for the problems, semi-empirical formulae are also limited to give an order of magnitude as they still have large uncertainty that allows only for preliminary analysis of the problem. In spite,



semi-empirical formulae are a fast and cheap way to assess the problem, they are also used in numerical models to account for different sediment transport mechanisms, taking advantage of the high precision in hydrodynamics, and can be used to design experimental set-ups for physical modelling.

Physical modelling of sediment transport involves important difficulties to scale sediment. To account for the bedload transport, the Shields parameter must be considered. Furthermore, for the suspended transport the sediment fall velocity also has to be properly scaled. These two conditions often require small grain sizes and densities for sediment in the model to reproduce both mechanisms together with the hydrodynamics. This can lead to prohibitive costs. On the other hand, this approach can provide precise results and, in some cases, one of the sediment transport mechanisms dominates being possible to scale attending only to that parameter. Physical modelling can be also used to gather data for numerical modelling validation or to develop semi-empirical formulae.

Numerical models for sediment transport are still in development stage. The earlier ones consisted in phase-resolving Boussinesq wave models, which did not have enough precision to properly solve the hydrodynamics in processes such as wave breaking or interaction with the structure, the main reason is that these models are depth averaged. Later, RANS models coupled with sediment transport were developed and provided better accuracy.

They can be used in combination with physical modelling by validating the numerical model with unscaled physical models and then applying them to real scale problems, so both physical mechanisms (suspended and bedload transports) can be reproduced at prototype scale. As explained before, some numerical models use semi-empirical formulae to compute sediment transport, this allows to reduce the computational effort but must be done carefully in order not to introduce excessive errors.

As sediment transport is highly influenced by hydrodynamic conditions, simple models are often not accurate enough for complex hydrodynamics and so happens with sediment transport due to its strong dependence in flow parameters. However, simple models can be accurate enough for some applications while having less computational cost. Therefore, depending on the complexity of the problem and the hydrodynamics involved, different numerical models can be used.

Some of these numerical models have been developed by including sediment transport in CFD (Computational Fluid Dynamics) software, the aim of this approach is to take advantage of the high precision that CFD offers to calculate the hydrodynamics. These models are also able to face the most complex situations. However, temporal scale of many of the scour is too large to be modeled with common CFD software in a reasonable time. For this reason, numerical models with the high precision of CFD software and able to solve the evolution of sediment in longer term (in a sea state for example) are demanded.

In this work, a 2D two-way coupled model for fluid-sediment interaction is developed. As hydrodynamic model, IH-2VOF is selected due to its capability to solve a sea state in reasonable time with high precision. The objective is to achieve a compromise between precision and computational effort and generate a useful tool for scour assessment and protection design in 2D configurations.



2. State of the art.

In this section, the currently available models which couple CFD with sediment transport in two-directional ways are discussed, focusing on Eulerian One-fluid models. Two-directional coupling consists in considering both the influence of hydrodynamics in sediment transport and the influence of sediment transport in hydrodynamics, this can be achieved with different strategies.

Firstly, these models can be classified attending to the nature of the considered sediment. Cohesive and non-cohesive sediments have different behavior as the firsts can flocculate in larger particles due to electrostatic forces. When flocs are transported, they can collide and break, warp or aggregate changing their properties. Because of the complexity of cohesive behavior and the applicability of non-cohesive models for most situations in maritime engineering, cohesive sediment models are not considered in this work.

There exist two main types of models to solve sediment transport equations depending on the approach:

- Eulerian models, that solve equations for sediment transport using a fixed mesh. These equations are applied to control volumes whose position relative to the coordinate axes is fixed. These methods use meshes to generate the control volumes.
- Lagrangian models, that solve the equations of motion (Newton's second law) for each particle considering the forces acting on it in which drag, lift or other forces generated by interaction with fluids can be included. In this case, the control volume moves with the particle or group of particles in some models. Lagrangian models can use a mesh to improve the efficiency of collision detection algorithms, but not to calculate the position of the sediment.

Other classification criterion is the number of phases in hydrodynamic model:

- One-fluid models, consider only one phase for water or other carrier fluid in the hydrodynamic model equations (mass and momentum conservation). There is no influence of sediment transport in the fluid equations. In spite, the fluid-sediment interaction can be introduced in other forms, typically by moving the boundaries of the domain and varying boundary conditions. There are only Eulerian models in this group. It is important to highlight that these models can use two or more different fluids in the hydrodynamics as in the case of multiphase solvers, but they do not consider the sediment phase in fluid equations.
- Two-fluids models, two phases are considered to model hydrodynamics, one for the carrier fluid and other for the sediment, this allows the model to better reproduce the fluid-sediment interaction. More phases could be considered, for instance, if water free surface is modeled. The position of the sediment phase can be computed with Lagrangian or Eulerian approach depending on the model.

In the figure below, a scheme resuming these classifications is presented.

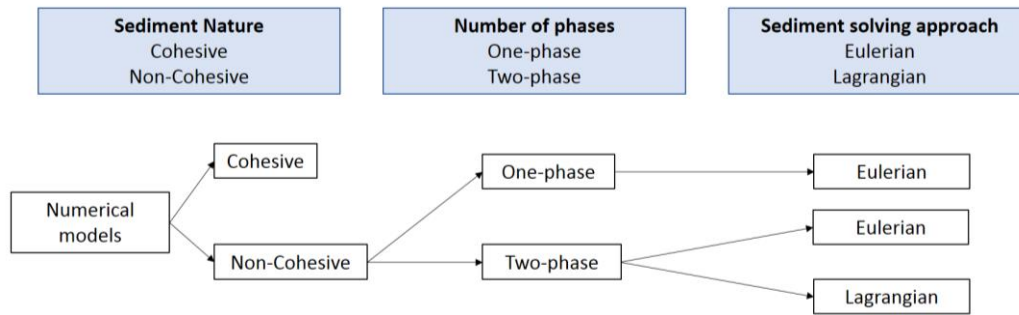


Figure 3: Classification of CFD models for sediment transport.

In most of the cases, fluid equations are solved using eulerian approach (such as Finite Volume Method), despite there exist some models which use Lagrangian approach, for instance Smoothed Particle Dynamics (SPH) models. For this reason, it is common to add “Eulerian” or “Lagrangian” before the sediment model to indicate the solving approach for hydrodynamics, which can be different from the one used to solve the sediment transport equations. In this work, only Eulerian approach for fluid solving is considered.

In the following content, Eulerian one-fluid models are described in depth as it is the type of numerical model developed in this work.

2.1. Eulerian One-fluid models description.

These models include three different sub-models to solve hydrodynamics, sediment transport and morphology. The overall structure of this models is depicted below.

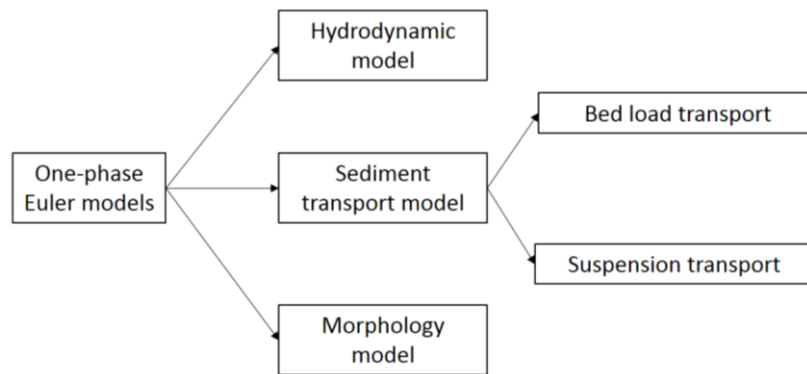


Figure 4: Structure of Eulerian One-fluid models.

Each model uses different equations, solving methods and mesh.

2.1.1. Hydrodynamic model.

The hydrodynamics are solved using Computational Fluid Dynamics (CFD), which typically solves a system of partial differential equations which are mass conservation and the Reynolds Averaged Navier-Stokes equations (RANS) with a turbulence closure model (typically $k - \omega$ or $k - \epsilon$). If free surface has to be considered, the most common technique used is the Volume Of Fluid method (VOF). Although solving RANS equations is the most usual approach for consultancy/industrial applications, Large Eddy Simulation models have also been used for this purpose. Other types of hydrodynamic model solve directly Navier-Stokes equations without turbulence modelling (Direct Numerical Simulation), however they are very expensive from a



computational point of view and, therefore, they are only used for specific applications beyond the scope of this work.

Firstly, from mass balance in a control volume, the mass conservation equation is obtained

$$\frac{\partial \rho}{\partial t} + \nabla \cdot (\rho \vec{u}) = 0 \quad \text{eq. 2.1}$$

Where ρ is the density of the fluid, and \vec{u} the velocity vector. Notice that, for constant density conditions (incompressible flows generally match this conditions), this equation collapses in

$$\nabla \cdot \vec{u} = 0 \quad \text{eq. 2.2}$$

Secondly, to obtain the Navier-Stokes equations, momentum balance is performed in control volume

$$\frac{\partial(\rho \vec{u})}{\partial t} + \nabla \cdot (\rho \vec{u} \otimes \vec{u}) = -\vec{\nabla} p + \nabla \cdot (\vec{\tau}) + \vec{S}_M \quad \text{eq. 2.3}$$

Here p is the pressure, $\vec{\tau}$ is the tangential stress tensor and \vec{S}_M is a term which can include various sources of body forces such as gravitational forces. \otimes denotes the outer product of two vectors, which is equivalent to a matrix multiplication of the shape $\vec{u} \otimes \vec{u} = \vec{u}\vec{u}^T$.

The second right-hand side term of this equation can be obtained from the viscous model of behavior. Following the Boussinesq hypothesis, the stress tensor is proportional to the strain rate tensor, the constant of proportionality is the dynamic viscosity (μ).

$$\vec{\tau} = 2\mu \vec{S} \quad \text{eq. 2.4}$$

Where \vec{S} is the strain rate tensor. Including this behavior model into momentum balance equations, Navier-Stokes equation results

$$\frac{\partial(\rho \vec{u})}{\partial t} + \nabla \cdot (\rho \vec{u} \otimes \vec{u}) = -\vec{\nabla} p + \nabla \cdot (2\mu \vec{S}) + \vec{S}_M \quad \text{eq. 2.5}$$

The strain rate tensor can be expressed in tensorial notation as

$$\vec{S} = \frac{1}{2} [\vec{\nabla} \vec{u} + (\vec{\nabla} \vec{u})^T] \quad \text{eq. 2.6}$$

Introducing the previous expression in the second right hand term of eq. 2.3

$$\nabla \cdot (2\mu \vec{S}) = \nabla \cdot (\mu [\vec{\nabla} \vec{u} + (\vec{\nabla} \vec{u})^T]) = \mu \nabla^2 (\vec{u}) + \nabla \cdot [\mu (\vec{\nabla} \vec{u})^T] \quad \text{eq. 2.7}$$

Expanding $\nabla \cdot [\mu (\nabla u)^T]$ an applying derivatives properties

$$\nabla \cdot [\mu (\vec{\nabla} \vec{u})^T] = \vec{\nabla} \mu (\vec{\nabla} \vec{u})^T + \mu \vec{\nabla} (\nabla \cdot \vec{u}) \quad \text{eq. 2.8}$$

Therefore, for isotropic ($\vec{\nabla} \mu = 0$) and constant density flow ($\nabla \cdot \vec{u} = 0$), the term $\nabla \cdot [\mu (\nabla u)^T]$ in eq. 2.6 becomes zero. Thus, if the fluid matches these assumptions the strain rate tensor can be simplified as



$$\bar{S} = \frac{1}{2} \vec{\nabla} \vec{u} \quad \text{eq. 2.9}$$

Including this in momentum balance equation and rearranging, the Navier-Stokes equation for constant density and isotropic fluids is obtained.

$$\frac{\partial(\rho \vec{u})}{\partial t} + \nabla \cdot (\rho \vec{u} \otimes \vec{u}) = -\vec{\nabla} p + \mu \nabla^2 \vec{u} + \vec{S}_M \quad \text{eq. 2.10}$$

However, to obtain the instantaneous value of the velocity vector can be computationally expensive because of the small-scale effect of the turbulence. For this reason, velocity vector is decomposed in a mean value and fluctuations, both affecting the momentum balance.

$$\vec{u} = \vec{U} + \vec{u}' \quad \text{eq. 2.11}$$

Where \vec{U} denotes the mean value of the velocity and \vec{u}' is the fluctuating velocity.

In fact, for most of the engineering applications there is no need to fully simulate turbulence. For this reason, rather than calculating the values of mean and instantaneous fluctuating velocities, equations can be averaged in time.

Notice that the average value of the mean velocity is the mean velocity itself and for velocity fluctuations the averaged value is assumed to be 0. However, the mean value of the product of two fluctuating velocities is not necessarily equal to 0, notice that the product of a velocity component by itself is never less than 0. For this reason, when the Navier-Stokes equations are time averaged, only the second term in the left-hand side of the equation includes the velocity fluctuations.

Considering this separation of the velocity vector in mean and fluctuating components and averaging in time, the following equation results.

$$\frac{\partial(\rho \vec{U})}{\partial t} + \nabla \cdot (\rho \vec{U} \otimes \vec{U}) + \nabla \cdot (\rho \vec{u}' \otimes \vec{u}') = -\vec{\nabla} p + \mu \nabla^2 \vec{U} + \vec{S}_M \quad \text{eq. 2.12}$$

The term including the velocity fluctuations effect is usually moved to the right-hand side and considered as a stress. The resulting equation is named Reynolds Averaged Navier-Stokes equation (RANS).

$$\frac{\partial(\rho \vec{U})}{\partial t} + \nabla \cdot (\rho \vec{U} \otimes \vec{U}) = -\vec{\nabla} p + \mu \nabla^2 \vec{U} - \nabla \cdot (\rho \vec{u}' \otimes \vec{u}') + \vec{S}_M \quad \text{eq. 2.13}$$

Some authors proposed ways to deal with fluctuating velocities. The most common is the Reynolds approach, in which fluctuating velocities are assumed to be proportional to the mean strain rate. The 2D tensor resulting from the cross product of fluctuating velocities is named Reynold's stress tensor.

$$\vec{u}' \otimes \vec{u}' = \bar{\tau}' = 2\mu_t \bar{S} \quad \text{eq. 2.14}$$

Notice the similarity between this expression and eq. 2.4. The constant value which relates velocity fluctuations and mean strain rate (μ_t) is named dynamic turbulent viscosity, and can also be expressed as kinematic viscosity

$$\nu_t = \frac{\mu_t}{\rho} \quad \text{eq. 2.15}$$



Including this assumption in RANS equation and following the same process as in Navier-Stokes equation for isotropic and incompressible fluids

$$\frac{\partial(\rho \vec{U})}{\partial t} + \nabla \cdot (\rho \vec{U} \otimes \vec{U}) = -\vec{\nabla} p + (\mu + \mu_t) \nabla^2 \vec{U} + \vec{S}_M \tag{eq. 2.16}$$

Turbulent viscosity is often higher than the molecular viscosity, in these cases turbulence treatment becomes important. To evaluate turbulent viscosity, turbulence models are needed.

Summarizing, Navier-Stokes equations along with mass conservation leads to a system of four partial differential equations (as Navier-Stokes equations are decomposed in one equation for each velocity component) with four variables (three velocity components and pressure). For problems with variable density and temperature, equation of energy transport and state equations (relating temperature, pressure and internal energy) are included resulting in seven equations with seven variables. RANS equations include turbulent viscosity which is calculated by the turbulence model, this model typically includes two extra variables and two extra equations.

The resulting system of equations can be solved only with numerical methods for a general case, although for simple configurations they can be simplified to a point where analytic solution can be obtained yielding widely used equations in Fluid Mechanics. Numerical methods used by CFD software aim to convert the system of partial differential equations in an algebraic system of equations, the selected method depends on the specific software, being the Finite Volume Method (FVM) the most common technique. CFD software commonly includes algorithms such as conjugated gradient and preconditioners to solve the system of algebraic equations in an efficient manner.

2.1.2. Sediment transport model.

In this model, two possible contributions for sediment transport are considered. First, the bed-load transport, which occurs next to the seabed due to different mechanisms (sliding, rolling and saltating), and second the suspended transport.

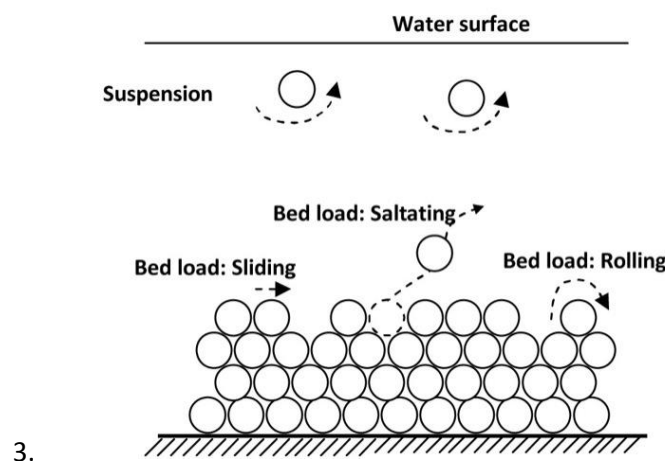


Figure 5: Sediment transport model with bed load mechanisms and suspended load transport. Image from <https://serc.carleton.edu/48147>

2.1.2.1. Bedload transport.

The aim of this model is to compute the bed load transport ($\overline{q_b}$). Later, its divergence will be obtained to calculate the variation in sediment volume inside each cell together with the suspended transport contribution, potentially resulting in a mesh movement.



Although different formulae are proposed for bedload transport, the one from (Roulund, et al., 2005) which extends (Engelund & Fredsoe, 1976) equations is usually applied in numerical models due to its simplicity:

$$\vec{q}_b = \frac{1}{6} \pi d^3 \frac{p_{EF}}{d^2} \vec{U}_b \quad \text{eq. 2.17}$$

In which d is the particle diameter, p_{EF} the percentage of particles in motion in the surface layer of the bed and \vec{U}_b the velocity of the moving particles. Thus, to calculate the bed load transport p_{EF} and \vec{U}_b must be obtained.

The percentage of particles is calculated with the following expression:

$$p_{EF} = \left[1 + \left(\frac{\frac{1}{6} \pi \mu_d}{\theta - \theta_c} \right) \right]^{-\frac{1}{4}} \quad \text{eq. 2.18}$$

Where μ_d is the dynamic friction coefficient of particles (typically 0.51 for sand), θ is the Shields parameter associated with skin friction and θ_c its critical value for bed motion initiation.

Critical Shields parameter is composed by a basic value (θ_{c0}) and a coefficient which accounts for the bed slope effect.

$$\theta_c = \theta_{c0} \left(\cos \beta \sqrt{1 - \frac{\sin^2 \alpha \tan^2 \beta}{\mu_s^2}} - \frac{\cos \alpha \sin \beta}{\mu_s} \right) \quad \text{eq. 2.19}$$

θ_{c0} is the critical Shield's parameter for horizontal bed, μ_s is the static friction coefficient (often considered as 0.63 for sand), β is the angle of the slope and α is the angle between velocity vector of the flow and the direction of the steepest bed slope.

Shield's parameter is computed as:

$$\theta = \frac{|\vec{U}_f|^2}{(s-1)gd} \quad \text{eq. 2.20}$$

In which $|\vec{U}_f|$ is norm of the friction velocity, s is the relative density and g the gravity acceleration. Friction velocity is the only variable which connects the bedload transport model with the hydrodynamic model, and depends on the tangential stress on the seabed ($\vec{\tau}_0$)

$$\vec{\tau}_0 = \rho \vec{U}_f^2$$

Tangential stress can be computed from velocity distribution next to the seabed. For example, in (Jacobsen, et al., 2014) the velocity distribution of (van Driest, 1956) is considered rather than calculated with the hydrodynamic model, as this increases the stability of the model and reduces the computational effort as boundary layer does not have to be calculated.

\vec{U}_b calculations are based on the equilibrium of an individual particle laying on the seabed, the relevant variables for this analysis are schemed in the following picture:

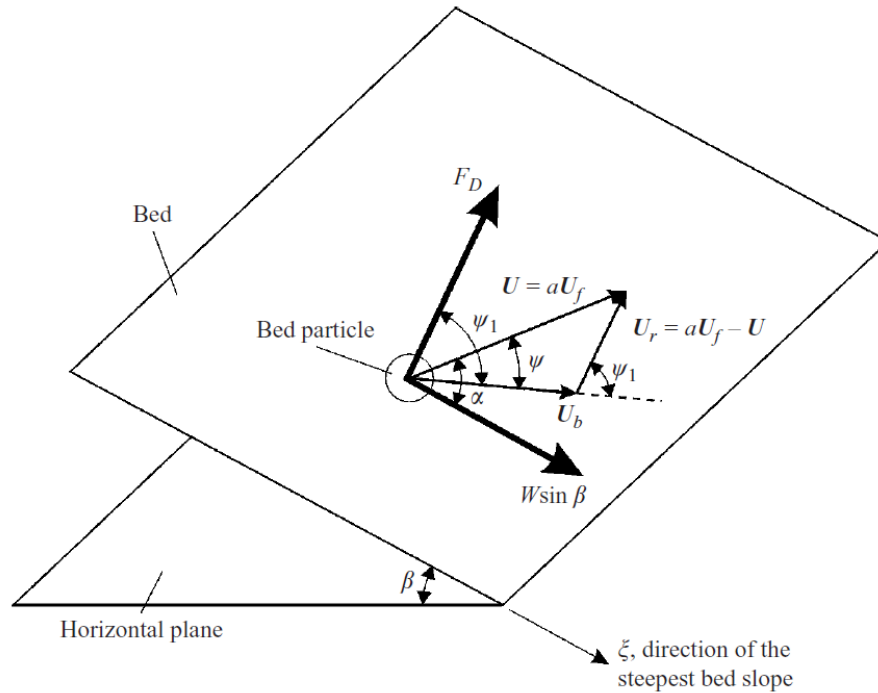


Figure 6: Geometry of forces and velocities on a seabed particle. Image from (Roulund, et al., 2005)

Fluid velocity at the position of the particle can be approximated from friction velocity as $\vec{U} = a\vec{U}_f$ where a is a coefficient, in (Roulund, et al., 2005) $a = 10$ is considered. Formulation also accounts for the angle between relative velocity and the velocity of the particle (ψ_1) and the angle between velocity of the flow and of the particle (ψ).

To determine the velocity of moving particles, stabilizing and agitating forces in parallel and perpendicular to \vec{U}_b directions acting on the particles and geometrical constrains are considered. The result is a system of four equations with four unknown variables.

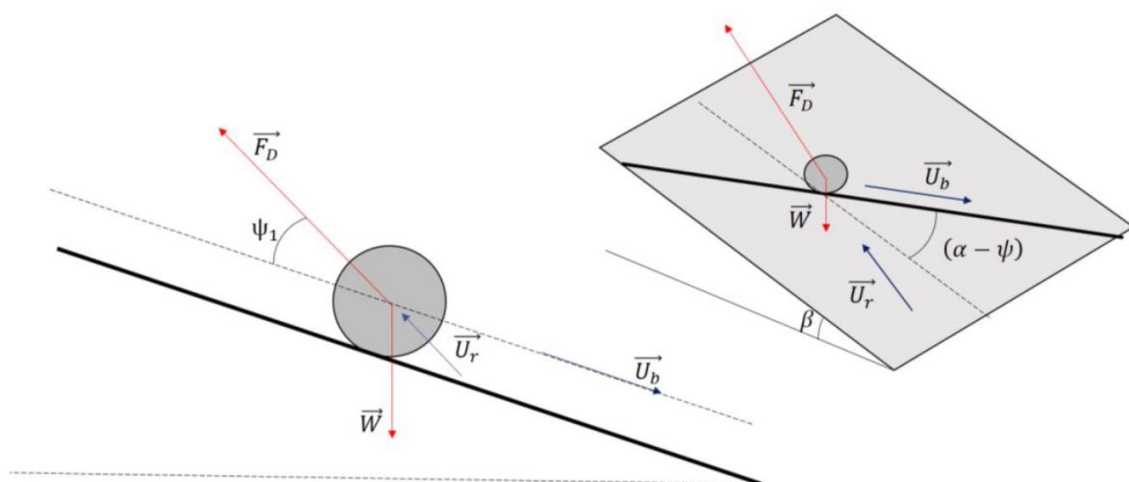


Figure 7: Forces acting on a seabed particle.

Forces balance parallel to \vec{U}_b



$$\vec{F}_D \cos \psi_1 + \vec{W} \sin \beta \cos(\alpha - \psi) - (\vec{W} \cos \beta) \mu_d = 0 \quad \text{eq. 2.21}$$

Forces balance perpendicular to \vec{U}_b

$$\vec{F}_D \sin \psi_1 - \vec{W} \sin \beta \sin(\alpha - \psi) = 0 \quad \text{eq. 2.22}$$

Geometric constrains

$$\vec{U}_r \sin \psi_1 - a \vec{U}_f \sin \psi = 0 \quad \text{eq. 2.23}$$

$$\vec{U}_r \cos \psi_1 - a \vec{U}_f \cos \psi + \vec{U}_b = 0 \quad \text{eq. 2.24}$$

Therefore, a four equations with four unknown variables (\vec{U}_r , \vec{U}_b , ψ and ψ_1) system of equations is obtained. Drag and lift effects are included in \vec{F}_D by using coefficient c :

$$\vec{F}_D = \frac{1}{2} \rho c \frac{\pi}{4} d^2 \vec{U}_r^2 \quad \text{eq. 2.25}$$

$$c = C_D + \mu_d C_L \quad \text{eq. 2.26}$$

Where C_D and C_L are the drag and lift coefficients of the particle. Coefficient c can be obtained in diverse ways, for example (Luque, 1974)

$$c = \frac{4\mu_s}{3a^2 \left(\frac{1}{2} \theta_{c0}\right)} \quad \text{eq. 2.27}$$

The weight of the particle can be calculated as

$$\vec{W} = \frac{1}{6} \pi \rho \vec{g} (s - 1) d^3 \quad \text{eq. 2.28}$$

At some points, the slope of the scour (β) could be close to the angle of repose (β_r) and, as a result, slides occur and a new slope for the bed results. Condition for slide is

$$\beta > \beta_r$$

In this situation, an iterative process is performed to reach a stable bed slope. The stable bed slope is

$$\beta < \beta_r$$

The iterative procedure to model the sand slide consists in the following 4 steps:

1. Determine zones where the slope exceeds the angle of repose. $\beta > \beta_r + 2^\circ$
2. Calculate the new sediment transport in this region based on a new particle velocity U_b computed from

$$\vec{W} \sin \beta - \mu_d \vec{W} \cos \beta - \frac{1}{2} \rho C_D \frac{\pi}{4} d^2 \vec{U}_b^2 = 0 \quad \text{eq. 2.29}$$

3. Update the bed morphology.



4. Repeat until the slope is reduced to $\beta_r - 2^\circ$

In this procedure, a pseudo time step is used as it is assumed that the sand slide occurs instantaneously. There is a margin of two degrees with respect to the angle of repose, this is done to increase the efficiency of the algorithm.

2.1.2.2. *Suspended sediment transport.*

Sediment can be eroded from seabed and can also be deposited on it; these processes constitute an interchange of sediment between the seabed and the fluid. To compute them, the sediment concentration at each point of the domain needs to be calculated. The transport of sediment inside the fluid domain is determined by the following advection-diffusion equation:

$$\frac{\partial c}{\partial t} = \nabla \cdot [(\alpha \vec{u} + \vec{w}_s)c] + \nabla \cdot [\alpha(\nu + \nu_t)\nabla c] \quad \text{eq. 2.30}$$

Where c is the sediment concentration, \vec{u} is the velocity vector, \vec{w}_s is the sediment fall velocity, α is the volume fraction of water (this ensures that if sediment enters the air fraction, it will fall fast following $\frac{\partial c}{\partial t} = \nabla \cdot (\vec{w}_s c)$) and ν and ν_t are the molecular and turbulent viscosities. ν is included because an advection problem is harder to solve numerically than a diffusion-advection one due to numerical instability, and this could happen if ν_t becomes 0. Notice that sediment diffusivity is considered equal to the momentum diffusivity, this means that Smith number (σ_c) is equal to one.

The sediment fall velocity for an isolated particle can be obtained from different formulae, for instance (Fredsoe & Deigaard, 1992)

$$\vec{w}_{s0} = \frac{(s-1)\vec{g}d^2}{18\nu} \quad \text{eq. 2.31}$$

However, a correction due to the interaction with the rest of the particles is needed. This correction must depend on the sediment concentration

$$\frac{|\vec{w}_s|}{|\vec{w}_{s0}|} = (1-c)^n \quad \text{eq. 2.32}$$

Where n is a function of parameter $\mathcal{R} = \frac{|\vec{w}_{s0}|d}{\nu}$

$$\begin{aligned} n &= 4.35\mathcal{R}^{-0.03} & \text{for } 0.2 < \mathcal{R} < 1 \\ n &= 4.45\mathcal{R}^{-0.10} & \text{for } 1 < \mathcal{R} < 500 \\ n &= 2.39 & \text{for } 500 < \mathcal{R} \end{aligned}$$

As sediment fall velocity depends on the sediment concentration, it must be calculated in the whole fluid domain.

The advective-diffusive transport equation can be solved fully implicit using the backward Euler time integration, suited for solving equations of the shape

$$\frac{\partial y}{\partial t} = f(y, t) \quad \text{eq. 2.33}$$



Which fits the advection-diffusion equation previously described, notice that in this case fluid variables are known as a result of hydrodynamics model for the corresponding cell. The method computes an approximation of y iterating for each time step (k) with a time interval (h)

$$y_{k+1} = y_k + h \cdot f(t_{k+1}, y_{k+1}) \quad \text{eq. 2.34}$$

Where $y_{k+1} = y_{t_0+kh}$ appears in both sides of the equation. To compute the unknown y_{k+1} the fixed-point iteration method can be used to obtain an approximated solution.

$$y_{k+1}^{[0]} = y_k \quad \text{eq. 2.35}$$

$$y_{k+1}^{[i+1]} = y_k + h \cdot f(t_{k+1}, y_{k+1}^{[i]}) \quad \text{eq. 2.36}$$

Where superscript i denotes the iteration.

This method is repeated several times per each time step of the hydrodynamic model. The reason for this is that the ratio between sediment fall velocity and the vertical velocity of the fluid is large next to the seabed (notice that sediment fall velocity is not explicitly affected by the presence of the boundary layer while flow velocities are) and this could lead to values of the Courant Number higher than 1 if the same time-step size is used for RANS. Thus, a smaller time-step size is needed to solve this equation.

Suspended load mesh uses part of the fluid mesh, removing cells which are closer to the seabed (in these cells the concentration is assumed to be constant). The distance from seabed in which cells are removed is δ_b and sediment concentration in this thin layer is called reference concentration (C_b), both are obtained from empirical formulae.

δ_b is commonly considered as two or three times the diameter of the particle, this can vary from different authors.

C_b can be obtained by using the following formulae

$$c_b = \frac{0.65}{\left(1 + \frac{1}{\lambda_b}\right)^3} \quad \text{eq. 2.37}$$

$$\lambda_b = \sqrt{\frac{\theta' - 0.3}{0.027s\theta'}} \quad \text{eq. 2.38}$$

Where λ_b is the linear concentration on the seabed and θ' is the Shield's parameter taking into account the effect of dunes. As the reference concentration can be calculated for each cell and assuming that cell size is sufficiently minor compared with the wavelength of the dunes, the effect of dunes is considered implicitly and therefore the Shield's parameter can be obtained with the previously described method. On the other hand, in (Engelund & Fredsoe, 1976) a constant value of $c_b = 0.32$ is proposed for sand sediments.



Once the concentration is known at each cell, erosion and deposition of sediment can be calculated with

$$\vec{E}_v = (v + v_t) \frac{\partial c}{\partial n} |\vec{N}| = (v + v_t) \vec{N} \nabla c \quad \text{eq. 2.39}$$

$$\vec{D}_v = c_b |(\vec{u} + \vec{w}_s) \vec{N}| \quad \text{eq. 2.40}$$

Where \vec{N} is a vector perpendicular to the cell surface and whose norm ($|\vec{N}|$) is equal to the cell area. Notice that the erosion (\vec{E}_v) is the diffusive flow of sediment projected in the direction perpendicular to the surface while \vec{D}_v is calculated as the sediment advective flow also projected to the surface normal direction.

The sediment volumetric flow due to erosion and deposition will be used together with the divergence of bedload transport to perform a mass balance in each seabed cell and determine the increment or decrement in sand level.

2.1.2. Morphology model.

Morphological changes occur when there is an inequilibrium between deposition, erosion and bed load transport. To obtain the variation in the height of each cell, a mass balance with these three contributions is performed.

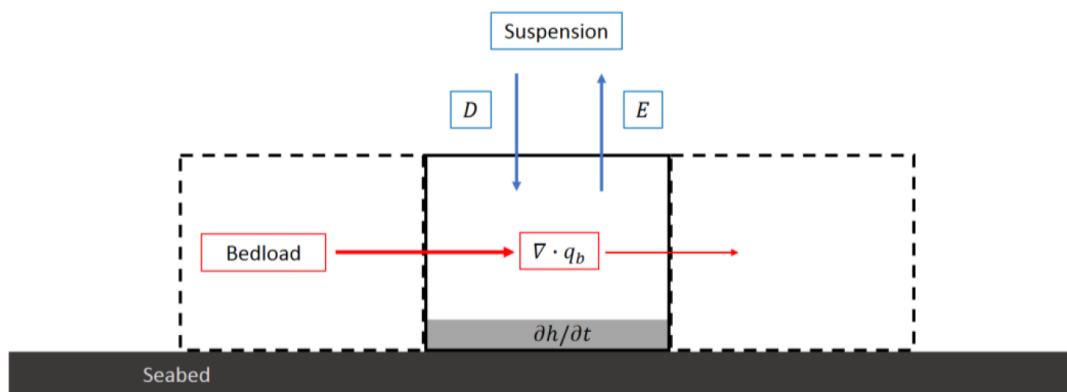


Figure 8: Sediment balance in seabed cell with contributions from bedload and suspended transport.

The level variation must be projected along vertical axis, as morphological updating is done only in this direction.

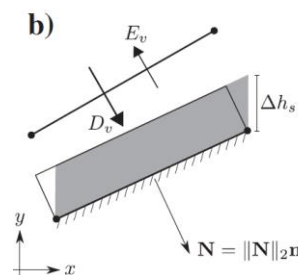


Figure 9: Balance for morphological changes. Image from (Jacobsen, et al., 2014)



Thus, the contribution from bedload transport is

$$\Delta h_b = -\frac{1}{1 - e_d} \frac{\nabla \cdot \vec{q}_b}{|\vec{n} \cdot \vec{e}_g|} \Delta t \quad \text{eq. 2.41}$$

Where \vec{n} is the unitary face-normal vector of the cell, \vec{e}_g is the unitary vector in vertical direction and e_d is the porosity of the seabed sediment.

The contribution from erosion and deposition is obtained with a similar expression

$$\Delta h_s = \frac{1}{1 - e_d} \frac{(|\vec{E}_v| + |\vec{D}_v|)}{|\vec{e}_g \cdot \vec{N}|} \Delta t \quad \text{eq. 2.42}$$

As previously stated, sediment balance allows to compute the amount of sediment accumulated into the cell in each time increment. Depending on how this time increment is, morphology models can be classified in:

Instantaneous models: Time increment for this model is equal to the time-step used to solve equations of the hydrodynamic model. In these models the total increment of height at each morphological time-step (Δt) is computed as

$$\Delta h = \Delta h_b + \Delta h_s \quad \text{eq. 2.43}$$

Time-averaged models: Time increment of morphology model is larger the time steps used to solve hydrodynamics equations, for instance, it can be equal to the wave period. To compute the variation in height for each morphological time-step the variations in the previous time-steps are considered by using the Adam-Bashforth third order explicit integration scheme.

$$\frac{\Delta \bar{h}^{i+1}}{\Delta t} = \frac{1}{12} (23\bar{F}^i - 16\bar{F}^{i-1} + 5\bar{F}^{i-2}) \quad \text{eq. 2.44}$$

Where \bar{F}^i is the time-averaged variation in seabed height in iteration i

$$\bar{F}^i = \frac{\Delta \bar{h}_b^i + \Delta \bar{h}_s^i}{\Delta t} \quad \text{eq. 2.45}$$

$\Delta \bar{h}_b^i$ and $\Delta \bar{h}_s^i$ are obtained using eq. 2.41 and eq. 2.42 with $\overline{\nabla \cdot \vec{q}_b}$, $|\overline{\vec{E}_v}|$, $|\overline{\vec{D}_v}|$, which are time-averaged in a time span equal to Δt .

For the morphology model, the mesh consists in dividing the seabed in areas, each of them can accumulate or lose sediment depending on the mass balance and varies its height accordingly. Thus, mesh for morphological model is a discretized surface which coincides with the seabed, this mesh is also used to obtain the divergence of bedload transport by using the Finite Area Method.

The description of Finite Area Method (FAM) is in (Tukovic & Jasak, 2012), it consists in the application of divergence theorem in two dimensions.

In general terms, the bidimensional divergence theorem considers an arbitrary vectorial field ($\vec{\Phi}$) defined on a surface S whose unitary normal vector is \vec{n} and curvature κ . The surface is

bounded by curve ∂S . To obtain the divergence of $\vec{\Phi}$ on the surface S the following equation can be used

$$\int_S \nabla_s \cdot \vec{\Phi} dS = \int_{\partial S} \vec{m} \cdot \vec{\Phi} dL - \int_S \kappa \vec{n} \cdot \vec{\Phi} dS \quad \text{eq. 2.46}$$

Where \vec{m} is the binormal vector, which is perpendicular to ∂S and tangent to S at all points of ∂S .

To solve this equation, the domain is discretized in control areas, whose area is S_{Af} . In the previous equation, integrals are substituted by summations

$$(\nabla_s \cdot \vec{\Phi})_{Af} = \frac{1}{S_{Af}} \sum_e \vec{m}_e \cdot \vec{\Phi}_e L_e - \kappa_{Af} \vec{n}_{Af} \vec{\Phi}_{Af} \quad \text{eq. 2.47}$$

Where subscript Af represents the control area and subscript e references the value at the middle point of the boundaries. The summation is done for all the edges which bound the control area Af .

The binormal vector at each boundary (\vec{m}_e) can be obtained with the following expression

$$\vec{m}_e = \vec{e} \times \frac{\vec{n}_i + \vec{n}_j}{|\vec{n}_i + \vec{n}_j|} \quad \text{eq. 2.48}$$

Where \vec{e} is the unitary vector parallel to the boundary and vectors \vec{n}_i and \vec{n}_j are the unitary normal vectors of surfaces which share the boundary.

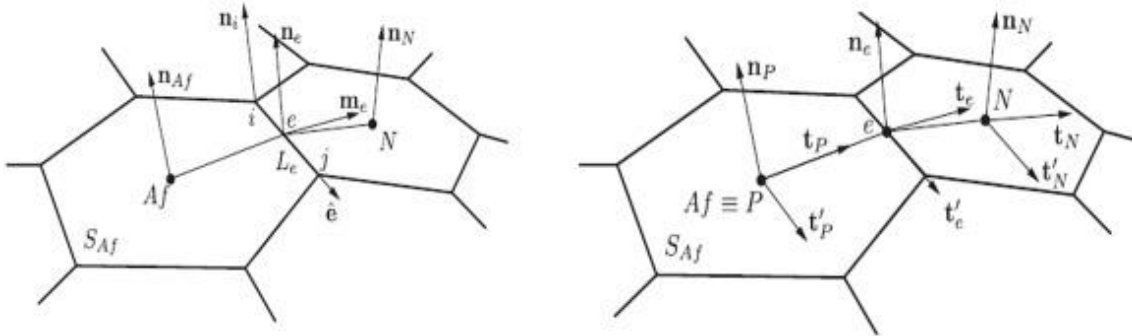


Figure 10: Control area at the deforming bed interface, a) general shape, and b) edge-based local orthogonal coordinate system. Image taken from Ahmed M.A. Sattar et al. (2017)

With eq. 2.47 the value of $\nabla_s \cdot \vec{\Phi}$ is known for each control area. However, to apply the discretized equations values of $\vec{\Phi}$ at the middle of the boundary are needed, this can be computed as

$$\vec{\Phi}_e = (T_e)^T \cdot [e_x T_P \vec{\Phi}_P + (1 - e_x) T_N \vec{\Phi}_N] \quad \text{eq. 2.49}$$

Where $\vec{\Phi}_P$ and $\vec{\Phi}_N$ are the values at the centre of each cell (which share the boundary) referred to the local coordinate system of its cells. T_e , T_P and T_N are the change of coordinates matrices from local coordinates at the boundary or cells to the global Cartesian system of coordinates. e_x is the distance between cell centres and the boundary.



The previously described theorem is applicable for calculating the divergence of bedload transport field $\nabla \cdot \vec{q}_b$ as the vector field \vec{q}_b is known, from bedload transport model, at each cell.

2.1.3. Coupling hydrodynamics and morphology models.

This coupling is achieved by moving the computational mesh of the fluid domain according to the already calculated morphology changes.

To do this, there are two possible approaches:

- **Pseudo-solid equations:** Mesh is treated as a solid with small deformations in a mechanical problem. An analogy with springs and torsional springs is used to compute changes in node positions.
- **Laplace equation:** solves the Laplace equation for the variable u_{mesh} which is the velocity of the moving mesh nodes.

In (Jasak & Tukovic, 2006) these possibilities are discussed. Pseudo-solid equations allow to compute mesh rotation by considering torsional springs but, on the other hand, they demand more computational resources. Finally, it is recommended to use the Laplace equation approach for sediment transport problems and for this reason only this method is briefly explained in this work.

Laplace equation for mesh moving is

$$\nabla(\gamma \nabla \vec{u}_{mesh}) = 0 \quad \text{eq. 2.50}$$

Where γ is the diffusion field which governs the mesh motion and \vec{u}_{mesh} is the velocity of mesh nodes. Once this equation is solved, the new position of each node of the mesh can be obtained as

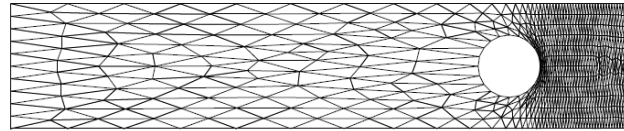
$$X_{new} = X_{old} + \vec{u}_{mesh} \Delta t \quad \text{eq. 2.51}$$

The value of γ can be computed with different strategies and it is important for the behaviour of the mesh. In this form of Laplace equation, a gradient of γ can be prescribed and, consistently with eq. 2.50, a gradient of mesh velocity will be generated to compensate it and satisfy the equation.

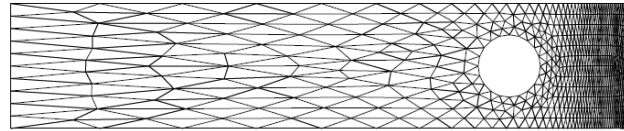
When moving mesh nodes, it is desirable to give more mobility to zones where mesh has to maintain high quality (such as solid boundaries where boundary layers have to be modelled). Consequently, γ must be higher in these zones of the domain.

For sediment transport problems, it is recommended to use distance-based methods in which γ is a function which decreases with the distance between cell centre and some selected boundary (in this case, the mobile bed), this decrease can be linear, quadratic or exponential depending on the implementation.

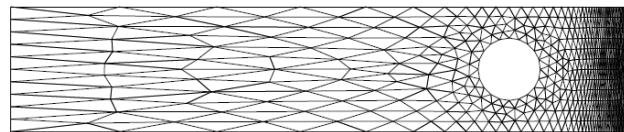
Other possible strategy is to compute the value of γ based on mesh quality indexes such as cell skewness or non-orthogonality.



(a) Constant.



(b) Linear distance-based (D1).

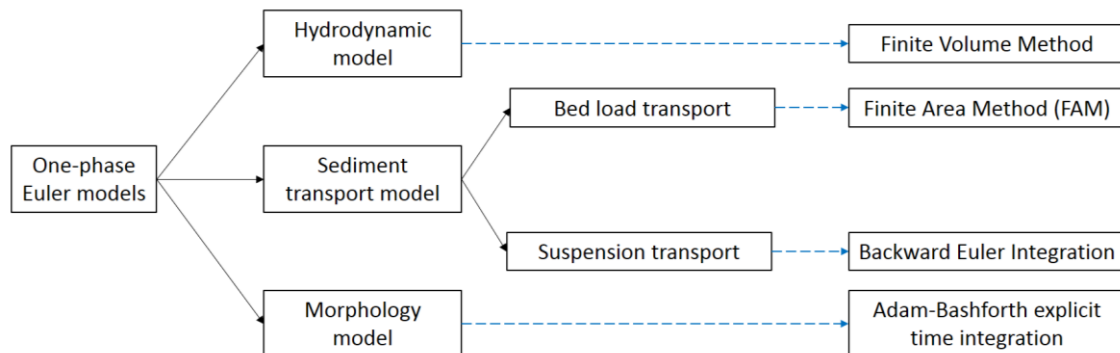


(c) Quadratic distance-based (D2).

Figure 11: Final mesh for a moving cylinder in a pipe with different gamma strategies. Image obtained from (Jasak & Tukovic, 2006)

2.1.4. Summary.

In the following scheme, models and its solving method are depicted.



For each model, a computational mesh is needed to solve its equations. As it has been explained, models use different equations and solving strategies, thus, different meshes are needed.

Models also have to share information. For instance, morphology model needs the bed load transport result but also erosion and deposition from suspended load transport to compute morphological changes.

In the following figure, meshes for each model and information shared between them is schemed.

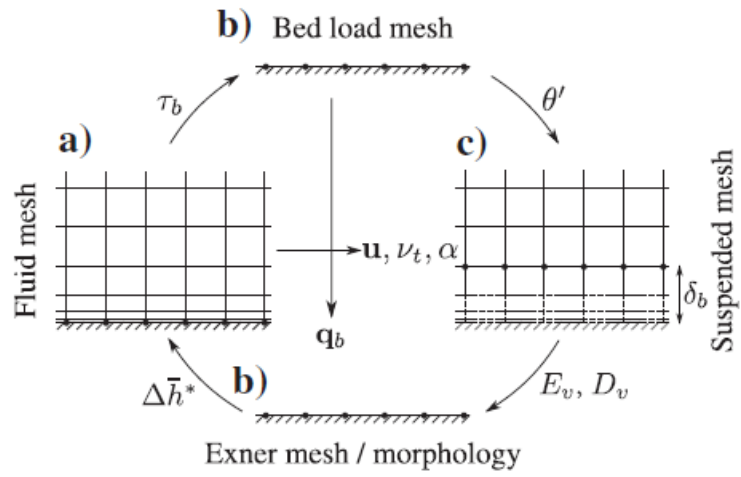


Figure 12: Different meshes used to solve components of the Eulerian model. Image taken from (Jacobsen, et al., 2014)



3. Implementation.

In the present work, a new sediment transport model is developed. To do this, IH-2VOF software from IHCantabria will be used as hydrodynamic model and new modules are included to account for sediment transport processes and seabed movement using an Eulerian One-Phase model.

As commented before, the main objective is to develop a fast and precise numerical model to predict sediment transport and bed morphology under different hydrodynamics.

The new models developed in this work are listed below and briefly explained.

- Bedload module: calculates bedload transport and its divergence at each cell on the seabed.
- Suspended load module: obtains the concentration of sediment at each cell in the fluid domain and the erosion/deposition on seabed.
- Sediment balance module: accounting for the volume of sediment entering each seabed cell by different mechanisms, this module obtains the increment or decrement in seabed height.
- Moving bed module: according to the previously calculated seabed position variation, this module fills or empties cells to adapt the actual seabed position in the numerical model, this allows to the interaction between flow and sediment.

Although this numerical model is based on the described method in section 2.1.2, as the hydrodynamic model differs from the one used in the reference paper, some modifications had to be done. These modifications will be described in following sections.

3.1. Hydrodynamic model.

Regarding the hydrodynamics, IH-2VOF has a different way to solve RANS equations than the common RANS solvers. Some of these aspects will be commented.

Firstly, IH-2VOF is a two-dimensional model, which means that some of the equations can be simplified.

Secondly, a finite difference method is used to compute the interpolated values of various magnitudes as well as for their derivatives, such as velocity and turbulent parameters. The results of this method will be latter used to compute the flux of the desired magnitude on each face cell and perform a balance in a similar way that for finite volume methods.

Lastly, IH-2VOF uses partial cell treatment to account for solid boundaries. This means that cells can be full of water, full of sediment or in an intermediate state, allowing to represent complex boundary shapes while using a simple structured cartesian mesh. This feature is desirable as it gives flexibility to the model allowing for large seabed displacements compared with traditional CFD software.

The process followed by the hydrodynamic model will be described in following content, its objective is to calculate the velocity and pressure fields. The velocity field will be used to drive both bedload and suspended sediment transport.

To obtain the velocity and pressure fields, this model uses the two-step projection method. Recall that the computed velocity and pressure field must satisfy RANS equations.



$$\frac{\partial(\rho\vec{U})}{\partial t} + \nabla \cdot (\rho\vec{U} \otimes \vec{U}) = -\vec{\nabla}p + (\mu + \mu_t)\nabla^2\vec{U} + \vec{S}_M \quad \text{eq. 3.1}$$

Considering RANS equations without the pressure term. For flows with constant density it can be expressed as

$$\frac{\partial(\vec{U})}{\partial t} = -\nabla \cdot (\vec{U} \otimes \vec{U}) + (v + v_t)\nabla^2\vec{U} + \vec{S}_M \quad \text{eq. 3.2}$$

This equation can be discretized in time to obtain an intermediate velocity field for the next time step (\tilde{U}^{n+1}):

$$\frac{\tilde{U}^{n+1} - \vec{U}^n}{\Delta t} = -\nabla \cdot (\vec{U}^n \otimes \vec{U}^n) + (v + v_t^n)\nabla^2\vec{U}^n \quad \text{eq. 3.3}$$

As pressure term has been extracted from this equation, the difference between the intermediate velocity and the velocity of next time step is

$$\frac{\vec{U}^{n+1} - \tilde{U}^{n+1}}{\Delta t} = -\frac{1}{\rho}\vec{\nabla}p^{n+1} \quad \text{eq. 3.4}$$

Where p^{n+1} denotes the pressure field in next time step. Now, considering the divergence of each side of previous expression

$$\nabla \cdot \left(\frac{\vec{U}^{n+1} - \tilde{U}^{n+1}}{\Delta t} \right) = \nabla \cdot \left(-\frac{1}{\rho}\vec{\nabla}p^{n+1} \right) \quad \text{eq. 3.5}$$

To satisfy continuity equation $\nabla \cdot (\vec{U}^{n+1}) = 0$, however this condition is not imposed for the intermediated velocity \tilde{U}^{n+1} , the previous equation yields

$$\frac{1}{\Delta t}\nabla \cdot (\tilde{U}^{n+1}) = \nabla \cdot \left(-\frac{1}{\rho}\vec{\nabla}p^{n+1} \right) \quad \text{eq. 3.6}$$

Which is named Poisson equation, commonly expressed in Einstein's notation as

$$\frac{\partial}{\partial x_i} \left(\frac{1}{\rho} \frac{\partial \tilde{U}^{n+1}}{\partial x_i} \right) = \frac{1}{\Delta t} \frac{\partial \tilde{U}^{n+1}}{\partial x_i} \quad \text{eq. 3.7}$$

Therefore, to obtain the pressure and velocity fields for time step n+1 first the intermediate velocity field \tilde{U}^{n+1} is obtained from eq. 3.3, then the pressure term for n+1 is given by eq. 3.7 and, finally, it is inserted in eq. 3.4 to obtain the velocity field for n+1.

To compute the two-step projection method, spatial derivatives of pressure and velocity are needed. As stated before, IH2VOF uses the finite difference method to obtain these derivatives. The spatial discretization of previous terms is not discussed in this work and the reader is referred to (Lin, 1998) for further information about the hydrodynamic model.

3.2. Bedload module.

The implementation of this module is quite similar to the one described in 2.1.2.1. Bedload transport. However, due to the differences between hydrodynamic modules, some



modifications had to be made on the original model. In this section, the most remarkable modifications will be described.

3.2.1. Friction velocity.

Recall that friction velocity is needed to compute the velocity of bed particles (\vec{U}_b). In IH-2VOF the boundary layer is approximated by using wall functions to gain efficiency. For this reason, the friction velocity is obtained assuming a logarithmic velocity profile next to solid boundary (turbulent boundary layer), the boundary layer is considered in a rough turbulent regime allowing to use Nikuradse's rugosity to obtain the vertical axis offset for the profile. With the previous considerations, the velocity profile is given by:

$$\frac{U_y}{U_f} = \frac{1}{\kappa} \text{Ln} \left(\frac{y}{K_s/30} \right) \quad \text{eq. 3.8}$$

Where U_y is the fluid velocity at a given position in vertical (y), κ is the von Karman's constant, K_s is the Nikuradse's rugosity (considered as three times the grain diameter) and U_f is the friction velocity.

In the previous formula, if a pair y , U_y inside the logarithmic profile is know, U_f can be determined. The values for y and U_y are obtained from the hydrodynamic model in the cell closest to the solid boundary, then, friction velocity is obtained from eq. 3.8 for each cell on the fluid-sediment interface.

3.2.2. Landslide mechanism.

When, at some point on the fluid-sediment interface, the slope exceeds the angle of repose of the material, landslide occurs. Modelling this phenomena in a proper manner is important as it represents a physical constrain in the seabed shape.

For this purpose, when the computed angle at some point of the interface exceeds the angle of repose by two degrees, the landslide cycle is activated and runs until the maximum slope is at least two degrees smaller than the angle of repose. This margin is considered to improve the efficiency of the sediment module.

The landslide mechanism is implemented as described in 2.1.2, therefore it will not be commented in this section. The slope of the fluid-sediment interface can be obtained from the position of the interface at each cell

$$\beta_i = \text{arctg} \left(\frac{yInter_i - yInter_{i-1}}{x_i - x_{i-1}} \right) \quad \text{eq. 3.9}$$

Where $yInter$ is the Y coordinate of fluid-sediment interface and subscript i denotes the cell index in X direction. $yInter$ is obtained by moving bed module.

3.2.3. Determining the velocity of particles.

Solving the system of equations previously described in 2.1.2 to obtain the particle's velocity for bedload transport requires the use of numerical methods such as Newton-Raphson algorithm. However, as in this case the model is two-dimensional, the system of equations can be simplified leading to a simple equation that can be solved explicitly to compute the velocity of moving particles.

Recalling the original system of equations



Forces balance parallel to \vec{U}_b

$$\vec{F}_D \cos \psi_1 + \vec{W} \sin \beta \cos(\alpha - \psi) - (\vec{W} \cos \beta) \mu_d = 0 \quad \text{eq. 3.10}$$

Forces balance perpendicular to \vec{U}_b

$$\vec{F}_D \sin \psi_1 - \vec{W} \sin \beta \sin(\alpha - \psi) = 0 \quad \text{eq. 3.11}$$

Geometric constrains

$$\vec{U}_r \sin \psi_1 - a \vec{U}_f \sin \psi = 0 \quad \text{eq. 3.12}$$

$$\vec{U}_r \cos \psi_1 - a \vec{U}_f \cos \psi + \vec{U}_b = 0 \quad \text{eq. 3.13}$$

In two-dimensions, the fluid velocity, drag force and weight are contained in the same plane, the velocity of the particle then has to be parallel to the fluid velocity vector. For this reason, angle $(\alpha - \psi)$ is equal to 0. Taking this into account, the force balance in direction perpendicular to \vec{U}_b becomes yields to $\sin \psi_1 = 0$, from the first geometric relation $\sin \psi = 0$ is deduced, then from forces balance parallel to \vec{U}_b the following equation is obtained

$$(\vec{W} \cos \beta) \mu_d = \vec{F}_D \quad \text{eq. 3.14}$$

Once \vec{F}_D is known, \vec{U}_r can be calculated and, applying the previous deductions in the second geometric constrain we obtain

$$\vec{U}_r - a \vec{U}_f + \vec{U}_b = 0 \quad \text{eq. 3.15}$$

From this equation \vec{U}_b can be calculated explicitly as \vec{U}_r and \vec{U}_f are already known.

3.3. Suspended transport module.

As explained before, IH-2VOF has a different strategy to solve RANS equations, based on a combination of finite differences and finite volumes methods. This is particularly important for solving the suspended transport governing equation, as it is related with the velocity field. In this section, several aspects of the implementation of this transport mechanism are described.

3.3.1. Solving advective-diffusive transport equation.

To solve the advective-diffusive transport equation for sediment concentration, the same combination of finite differences and finite volumes as in hydrodynamic model is used. This method is formulated as follows. R

First, the advective-diffusion equation for sediment transport (eq. 2.30), it can be integrated in each cell to obtain the total increment of concentration inside the cell

$$\oint_v \frac{\partial c}{\partial t} dV = \oint_v \nabla \cdot [(\alpha \vec{u} + \vec{w}_s) c] dV + \oint_v \nabla \cdot [\alpha (v + v_t) \vec{\nabla} c] dV \quad \text{eq. 3.16}$$

At this point, Gauss divergence theorem is applied, which converts the integral of the divergence of a certain tensor field over the volume to an integral of the field over the bounding surface.



$$\oint_v \nabla \cdot (\vec{f}) dV = \oint_s \vec{f} dS$$

Resulting in the following expression for eq. 3.16

$$\oint_v \frac{\partial c}{\partial t} dV = \oint_s c(\alpha \vec{u} + \vec{w}_s) dS + \oint_s \alpha(v + v_t) \vec{\nabla} c dS \quad \text{eq. 3.17}$$

As sediment concentration is assumed to be constant inside each cell, its integral in cell volume is

$$\oint_v \frac{\partial c}{\partial t} dV = \frac{\partial c}{\partial t} V_{cell} \quad \text{eq. 3.18}$$

And back to eq. 3.17

$$\frac{\partial c}{\partial t} V_{cell} = \oint_s c(\alpha \vec{u} + \vec{w}_s) dS + \oint_s \alpha(v + v_t) \vec{\nabla} c dS \quad \text{eq. 3.19}$$

In the hydrodynamic model, the mesh is structured and cartesian therefore it consists in rectangular cells. The value of sediment concentration, sediment gradient and velocities are constant on cell faces, for this reason, the integral over the cell surface can be transformed into summations.

For advective flux, the integral in eq. 3.19 becomes

$$\oint_s c(\alpha \vec{u} + \vec{w}_s) dS = \sum_n c_n (\alpha \vec{u}_n + \vec{w}_{s,n}) A_n$$

And for diffusive flux

$$\oint_s \alpha(v + v_t) \vec{\nabla} c dS = \sum_n \vec{\nabla} c_n (v + v_{t,n}) A_n$$

And eq. 3.19 results, moving the cell volume to the right-hand side in

$$\frac{\partial c}{\partial t} = \frac{\sum_n c_n (\alpha \vec{u}_n + \vec{w}_{s,n}) A_n + \sum_n \vec{\nabla} c_n (v + v_{t,n}) A_n}{V_{cell}} \quad \text{eq. 3.20}$$

Where subscript n denotes the face cell, A_n is the face cell area and V_{cell} is the cell volume

The derivative of sediment concentration with respect to the time will be discretized later using the previously described Backward Euler time integration method.

Therefore, for each cell in fluid domain, the mass fluxes on each face cell has to be computed and the variation in sediment concentration is obtained from eq. 3.20. The sign criterion for fluxes is schemed in the following figure

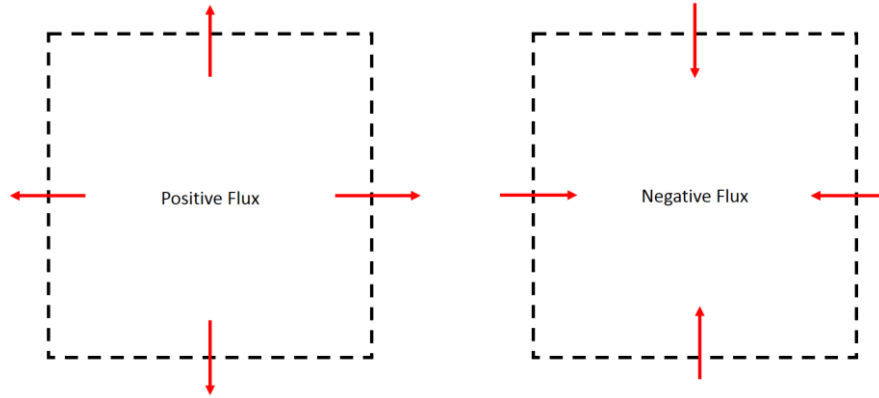


Figure 13: Sign criteria for fluxes on cell faces.

The reason to adopt this criterion is that fluxes are commonly calculated multiplying by the face normal unitary vector, which points out of the cell, resulting in positive values when the flux goes out of the cell. Although in this case it is not necessary to project the fluxes in the normal direction of the cells (as the mesh is cartesian), this criterion is conserved.

As the model is two-dimensional, only four fluxes have to be calculated for each cell with indexes i, j . The advective and diffusive contributions are calculated separately in the following way:

$$\left[\sum_n c_n (\alpha \vec{u}_n + \vec{w}_{s,n}) A_n \right]_{i,j} = FluxTAdv_{i,j} + FluxBAdv_{i,j} + FluxRAdv_{i,j} + FluxLAdv_{i,j} \quad eq. 3.21$$

$$\left[\sum_n \vec{v} c_n (v + v_{t,n}) A_n \right]_{i,j} = FluxTDiff_{i,j} + FluxBDiff_{i,j} + FluxRDiff_{i,j} + FluxLDiff_{i,j} \quad eq. 3.22$$

Where the fluxes are denoted with T, B, R, or L referring to Top, Bottom, Right or Left cell face and Adv or Diff for advective or diffusive respectively.

It is important to highlight that, as this model is dealing with partial cell treatment, the cell volume is not constant but depends on the value of coefficient AC.

$$V_{cell} = \Delta x_i \Delta y_j AC_{i,j}$$

Where Δx_i is the dimension of the cell in x direction and Δy_j in y direction. Recall that, as the mesh is cartesian, all cells in the same column have equal Δx_i and all cells in the same row have equal Δy_j . The fact that $AC_{i,j}$ is present in the calculations of cell volume can be problematic, as when cells at fluid-sediment interface get filled AC value can get close to 0, leading to numerical instabilities when eq. 3.20 is computed.

3.3.2. Interpolation of magnitudes.

At this point, interpolated values of different magnitudes need to be obtained at cell faces. The subscript notation which will be used in following content is schemed below.

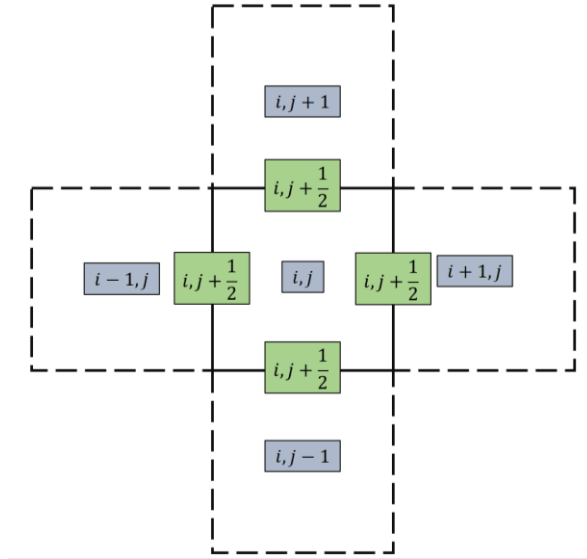


Figure 14: Cell and face indexes for interpolations. Blue squares represent cell indexes and green squares represent face indexes.

To obtain the fluxes on cell faces due to advective transport, the sediment concentration on the cell face is obtained by interpolation using a central difference scheme.

$$C_{i,j+\frac{1}{2}} = \frac{C_{i,j} + C_{i,j+1}}{2}$$

$$C_{i,j-\frac{1}{2}} = \frac{C_{i,j} + C_{i,j-1}}{2}$$

$$C_{i+\frac{1}{2},j} = \frac{C_{i,j} + C_{i+1,j}}{2}$$

$$C_{i-\frac{1}{2},j} = \frac{C_{i,j} + C_{i-1,j}}{2}$$

The fluid velocity value is already in cell faces, so interpolation is not needed for this magnitude.

To compute the diffusive flux, concentration gradient and turbulent viscosity must be obtained at each cell face. Spatial derivatives of concentration are obtained in finite difference form

$$\left(\frac{\partial C}{\partial x}\right)_{i+\frac{1}{2},j} = \frac{C_{i+1,j} - C_{i,j}}{\Delta x}$$

$$\left(\frac{\partial C}{\partial x}\right)_{i-\frac{1}{2},j} = \frac{C_{i,j} - C_{i-1,j}}{\Delta x}$$

$$\left(\frac{\partial C}{\partial y}\right)_{i,j+\frac{1}{2}} = \frac{C_{i,j+1} - C_{i,j}}{\Delta y}$$

$$\left(\frac{\partial C}{\partial y}\right)_{i,j-\frac{1}{2}} = \frac{C_{i,j} - C_{i,j-1}}{\Delta y}$$

The turbulent viscosity is interpolated in the same way as sediment concentration



$$v_{t,i,j+\frac{1}{2}} = \frac{v_{t,i,j} + v_{t,i,j+1}}{2}$$

$$v_{t,i,j-\frac{1}{2}} = \frac{v_{t,i,j} + v_{t,i,j-1}}{2}$$

$$v_{t,i+\frac{1}{2},j} = \frac{v_{t,i,j} + v_{t,i+1,j}}{2}$$

$$v_{t,i-\frac{1}{2},j} = \frac{v_{t,i,j} + v_{t,i-1,j}}{2}$$

And the VOF function ($F_{i,j}$), representing the relation between the amount of water and air inside the cell also has to be interpolated to satisfy mass conservation, this denomination is used inside IH2VOF code and corresponds to α in eq. 3.21.

$$F_{i,j+\frac{1}{2}} = \frac{F_{i,j} + F_{i,j+1}}{2}$$

$$F_{i,j-\frac{1}{2}} = \frac{F_{i,j} + F_{i,j-1}}{2}$$

$$F_{i+\frac{1}{2},j} = \frac{F_{i,j} + F_{i+1,j}}{2}$$

$$F_{i-\frac{1}{2},j} = \frac{F_{i,j} + F_{i-1,j}}{2}$$

Velocities do not have to be interpolated as their values are already for cell faces, velocity vector is given by its components, being $u_{i,j}$ the velocity in X direction on the right cell face and $v_{i,j}$ the velocity in Y direction on the top cell face.

With these interpolated values, fluxes for advective transport from eq. 3.21 are computed as:

$$FluxTAdv_{i,j} = C_{i,j+\frac{1}{2}} \left(F_{i,j+\frac{1}{2}} v_{i,j} + \overrightarrow{w_{s,l,j+\frac{1}{2}}} \right) \Delta x_i$$

$$FluxBAdv_{i,j} = C_{i,j-\frac{1}{2}} \left(F_{i,j-\frac{1}{2}} v_{i,j-1} + \overrightarrow{w_{s,l,j-\frac{1}{2}}} \right) \Delta x_i$$

$$FluxRAdv_{i,j} = C_{i+\frac{1}{2},j} \left(F_{i+\frac{1}{2},j} \overrightarrow{u_{i,j}} + \overrightarrow{w_{s,l+\frac{1}{2},j}} \right) \Delta y_i$$

$$FluxLAdv_{i,j} = C_{i-\frac{1}{2},j} \left(F_{i-\frac{1}{2},j} u_{i-1,j} + \overrightarrow{w_{s,l-\frac{1}{2},j}} \right) \Delta y_i$$

And for diffusive transport from eq. 3.22:

$$FluxTDiff_{i,j} = \left(\frac{\partial C}{\partial x} \right)_{i,j+\frac{1}{2}} \left(v + v_{t,i,j+\frac{1}{2}} \right) \Delta x_i$$

$$FluxBDiff_{i,j} = \left(\frac{\partial C}{\partial x} \right)_{i,j-\frac{1}{2}} \left(v + v_{t,i,j-\frac{1}{2}} \right) \Delta x_i$$

$$FluxRDiff_{i,j} = \left(\frac{\partial C}{\partial y} \right)_{i+\frac{1}{2},j} \left(v + v_{t,i+\frac{1}{2},j} \right) \Delta y_j$$



$$FluxLDiff_{i,j} = \left(\frac{\partial C}{\partial y} \right)_{i-\frac{1}{2},j} \left(v + v_{t_{i-\frac{1}{2},j}} \right) \Delta y_j$$

Where Δx_i and Δy_i are the cell horizontal and vertical directions respectively. Notice that these dimensions are not considered as constant, allowing for different mesh refinement in distinct regions of the fluid domain to gain efficiency.

3.3.3. Boundary conditions.

Boundary conditions for suspended sediment transport can be prescribed in different ways depending on the case. For instance, it can be a fixed value of concentration (Dirichlet condition), a fixed gradient (Neumann condition) or a combination of both (Cauchy condition) on the boundary. The boundary condition on fluid-sediment interface is more complex and for this reason will be described in depth.

The interchange of sediment volume between fluid domain and soil is conceptualized as represented in the following scheme:

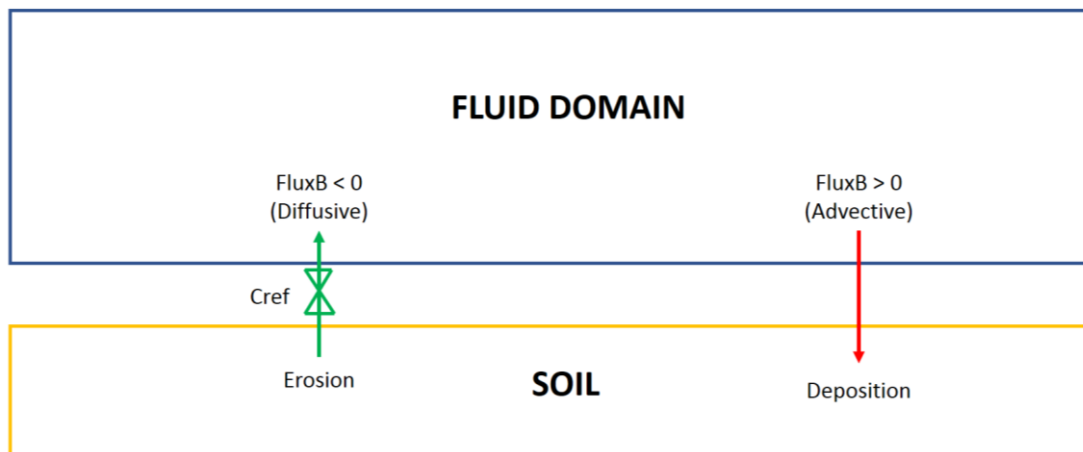


Figure 15: Schematic representation of sediment interchanges between fluid domain and soil.

Two separate ways of interaction are considered.

- Erosion: sediment extracted from the soil enters the fluid domain as diffusive flux on the bottom face of the interface cell. This process is controlled by the reference concentration as will be explained before.
- Deposition: sediment exits the fluid domain via advective flux on bottom face of the interface cell.

In this implementation, the reference concentration is not imposed in any cell in contrast with other models. This is done because imposing a certain value of concentration can lead to mass conservation problems. Taking this into account, interface cells are treated as regular cells when calculating the sediment concentration, however, the diffusive fluxes on cell faces are controlled by the following expressions for concentration gradient rather than the previously described one for general cells:

$$\left(\frac{\partial C}{\partial y} \right)_{i,j-\frac{1}{2}} = \frac{C_{i,j} - C_{ref,i}}{\Delta y}$$



Where $C_{ref,i}$ denotes the reference sediment concentration in position “ i ” of the fluid-sediment interface. This reference concentration is obtained with eq. 2.37 and eq. 2.38, however, the theoretical limit for $C_{ref,i}$ is set to 0.32 as suggested in (Engelund & Fredsoe, 1976). The resulting formulae is:

$$C_{ref,i} = \frac{0.32}{\left(1 + \frac{1}{\lambda_{b,i}}\right)^3} \quad \text{eq. 3.23}$$

$$\lambda_{b,i} = \sqrt{\frac{\theta_i - 0.3}{0.027s\theta_i}} \quad \text{eq. 3.24}$$

Notice that the limitation of 0.32 is imposed by the numerator in eq. 3.23. The value of Shields parameter at each position of the interface is obtained by the bedload transport model, being the connection between suspended and bedload transport.

Sediment interchanges in opposite directions are not allowed, thus, in this boundary condition positive diffusive fluxes and negative advective fluxes are set to zero.

As other possible uncontrolled interchanges between soil and fluid are not allowed, the diffusive flux on right or left faces is restricted in case that the cell aside is below the interface. Advective flux is not restricted explicitly for this situation, however, as the filled cell cannot have any incoming flow, this transport is also restricted.

The resulting possible flows are summarized in the following figure:

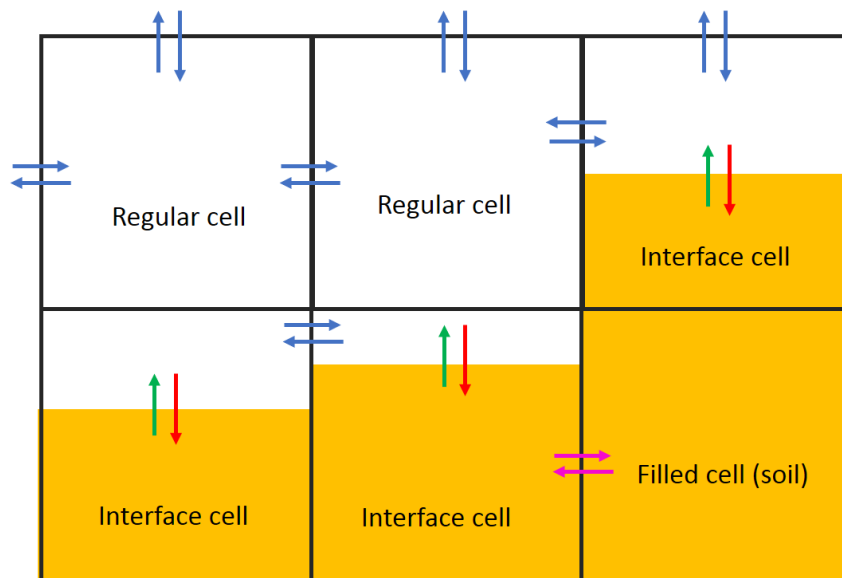


Figure 16: Schematic representation of boundary condition for fluid-sediment interphase and sediment flow restrictions. Regular sediment fluxes are depicted in blue, erosion and deposition fluxes in green and red respectively, the not-allowed flow between soil and interface cell is in magenta.

Once fluxes on each face are known, they must be integrated in time to obtain the variation in sediment concentration. To do this, Backward Euler time integration method is used. This technique has already been explained, in this implementation is applied as follows.



The hydrodynamic solver time step is divided in smaller time steps to solve the suspended transport, this is achieved by iterating several times for each fluid step (subcycles). Recalling eq. 2.35 and eq. 2.36, the first uses the concentration field from previous fluid time-step to compute the fluxes and update the concentration for the next subcycle:

$$C_{k+1}^{[0]} = C_k \quad \text{eq. 3.25}$$

$$C_{k+1}^{[it+1]} = C_k + \Delta t_{susp} \cdot \left[\frac{\sum_n c_n (\alpha \vec{u}_n + \vec{w}_{s,n}) A_n + \sum_n \vec{\nabla} c_n (v + v_{t,n}) A_n}{V_{cell}} \right]^{[it]} \quad \text{eq. 3.26}$$

Where superscript it indicates that the values are from actual iteration and $it + 1$ that they are for the next iteration, Δt_{susp} is the suspended transport time-step which can be obtained as

$$\Delta t_{susp} = \frac{\Delta t}{nSubcycles}$$

Notice that in eq. 3.26 velocity, turbulent viscosity and α fields are constant since they are updated every hydrodynamic time-step.

Finally, the same volume of sediment which enters the flow has to be taken from the soil. To obtain this volume the variation in sediment concentration in fluid cells is multiplied by the cell volume. Thus, erosion and deposition can be obtained also applying the time integration method as:

$$E_i^{[i+1]} = E_i^{[i]} - \Delta t_{susp} (FluxBDiff_{i,j} \cdot \Delta x_i \Delta y_j A C_{i,j})^{[i]} \quad \text{eq. 3.27}$$

$$D_i^{[i+1]} = D_i^{[i]} + \Delta t_{susp} (FluxBAdv_{i,j} \cdot \Delta x_i \Delta y_j A C_{i,j})^{[i]} \quad \text{eq. 3.28}$$

These eroded and deposited volumes will be used in sediment balance module to obtain the variation in fluid-sediment interface position.

3.4. Sediment balance module.

Once both bedload and suspended load contributions are computed, a sediment balance must be performed to determine the variation in sediment-fluid interface at each point. In this balance, the porosity of the cell is also considered.

Knowing the divergence of bedload transport, erosion and deposition rates, the increment of height for each interface cell is

$$\Delta h_i = \frac{1}{(1-p)} \frac{(\nabla \cdot \vec{q}_{bl})_i \Delta t + D_i - E_i}{\Delta x_i} \quad \text{eq. 3.29}$$



However, if Δh_i is assigned in this way, it tends to generate peaks on the interface. For this reason, its value is smoothed using different techniques. In this implementation, Gaussian averaged values are used like in (Peng, et al., 2018):

$$\Delta h_i = 0.1\Delta h_{i-2} + 0.2\Delta h_{i-1} + 0.4\Delta h_i + 0.2\Delta h_{i+1} + 0.1\Delta h_{i+2} \quad \text{eq. 3.30}$$

Finally, the increment of height at each position needs to be corrected. The reason is that, as the fluid-sediment interface raises, it occupies a fluid volume which has some sediment concentration on it as schemed in the following figure:

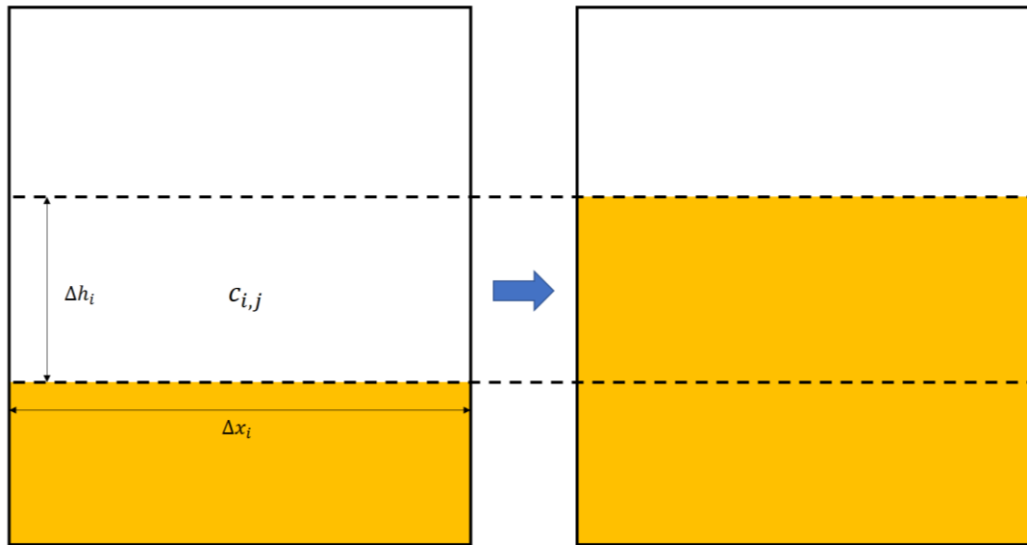


Figure 17: Volume of fluid occupied by an increment in fluid-sediment interface height.

If this correction is not performed, that amount of concentration is eliminated and, therefore, mass conservation is not satisfied. To solve this problem, the volume of sediment contained in the space occupied by the new position of the interface is computed as an extra increment of height:

$$\Delta h_i = \Delta h_i + \frac{c_{i,j}\Delta h_i}{(1-p)} \quad \text{eq. 3.31}$$

This operation should be repeated several times until Δh_i reaches a stable value, however, in this implementation only one iteration is enough to obtain acceptable results, as will be proved for example in test case 1.

Another issue involving mass concentration and fluid-sediment interface changes is that, when a new cell is opened, its concentration must be set to zero, in other case it would be creating mass artificially. This can generate discontinuities in sediment concentration field, however, the implementation has been proved to be robust enough to handle this problem.

3.5. Moving bed module.

The previously determined variation in seabed is applied in this module, in such a way that hydrodynamics will be modified as the lower boundary of the domain changes. Consequently,



this module adds to the hydrodynamics the influence of sediment transport, resulting in a two-way coupled sediment-fluid interaction model.

To do this, it is important to understand how does the lower boundary condition work in IH-2VOF. As discussed before, IH-2VOF uses partial cell treatment to be able to consider relatively complex shapes without generating serrated edges. In partial cell treatment, the following parameters are considered to solve the hydrodynamics in each cell when the it is located on a solid boundary:

- AC: relation between cell volume occupied by fluid and solid, $AC_{i,j} = 1$ means that the cell is full of fluid while $AC_{i,j} = 0$ indicates that it is full of sediment.
- AR: relation between opened and closed length of the right face of the cell. , $AR_{i,j} = 1$ means that the right side of the cell is fully opened while , $AR_{i,j} = 0$ indicates that it is completely closed.
- AT: relation between opened and closed length of the top side of the cell, it is equivalent to $AR_{i,j}$ but for the top face of the cell.
- NOC: indicates if the cell is part of an obstacle or not. $NOC_{i,j} = 0$ means that the cell does not intersect with any obstacle and $NOC_{i,j} = 1$ that it does.

From sediment balance module, the variation in fluid-sediment interface is known for each fluid time-step, and the partial cell parameters can be obtained from it. For fluid cells these parameters are:

$$AC_{i,j} = AR_{i,j} = AT_{i,j} = 1$$

$$NOC_{i,j} = 0$$

For cells full of sediment (under the interface):

$$AC_{i,j} = AR_{i,j} = AT_{i,j} = 0$$

$$NOC_{i,j} = 1$$

And for interface cells

$$AR_{i,j} = 0.5 + \frac{(Y_{center_{i,j}} - Y_{inter_i})}{Y_{j+1} - Y_j}$$

$$AC_{i,j} = AR_{i,j}$$

$$AT_{i,j} = 1$$

$$NOC_{i,j} = 1$$

Where $Y_{center_{i,j}}$ is the y coordinate at cell center and Y_{inter_i} is the y coordinate of the interface. The position of the interface is updated every hydrodynamic time-step by adding the previously obtained Δh_i for each cell.

$$Y_{inter_{i_{k+1}}} = Y_{inter_{i_k}} + \Delta h_{i_k}$$

Where subscript k denotes the actual time-step and $k + 1$ the next time-step.



Therefore, the initial position of the fluid-sediment interface must be obtained at the beginning of the simulation and it will be updated in successive time-steps. The algorithm to obtain the initial position consist in detecting the last cell with $AC_{i,j} < 1$ for each cell column.

In addition to partial cell parameters, velocity and turbulent viscosity values must be given to new fluid cells. The assigned values are the same as in the top side cell, the reason for this is to not generate discontinuities which can lead to instabilities in the hydrodynamic model.



4. Model test.

In this chapter, three tests are carried to check if the previously described numerical model is working properly.

These tests are intended to be a first step in the validation process, which will be described in chapter 5, allowing to detect issues with different sediment transport mechanisms. The results of these test cases can be easily calculated with analytically and, in some cases, tested by visual analysis of different plots.

Each test case is designed to give insight about either advective sediment transport, suspended sediment transport or landslide mechanisms.

4.1. Test case 1: sedimentation.

In this case, a simple sedimentation process is simulated. The case set-up consists in a reservoir of 3.5 meters high and 3 meters wide with calm water inside, the water free surface is at 3 meters from the bottom. The initial concentration is set to 0.1 (volumetric concentration) in the whole reservoir (including water and air) to check the behavior of the model also in the air.

For this test, it is interesting to analyze only the advective processes of sediment transport, allowing to detect problems in this mechanism such as mass conservation issues and numerical diffusions. For this reason, diffusive transport has been deactivated for this simulation.

Once the simulation starts, the sediment settles, and the fluid-sediment interface raises to an expected position of 0.35 m from the reservoir floor.

The total mass concentration is monitored during the simulation, although the mass conservation can also be checked with the final position of sediment interface.

The results of this test case are:

- Tracking of the position of fluid-sediment interface. As the sediment fall velocity is constant, the interface must raise at constant speed. The final position of fluid-sediment interface is also represented together with its expected position.
- Sediment concentration field. In this case, it has been obtained every 100 seconds and represented in a contour plot to give an idea of the evolution of sediment concentration along the test.

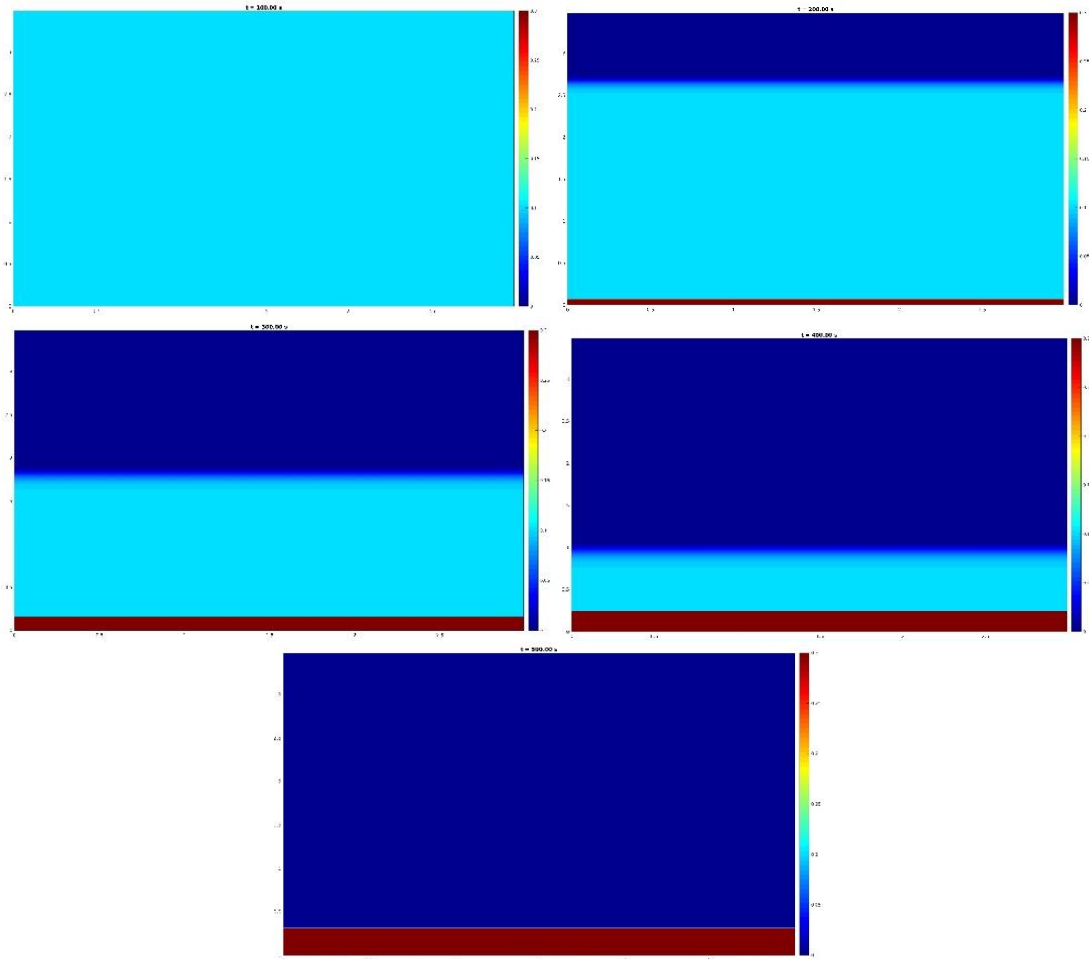


Figure 18: Sediment concentration contour plots at each 100 seconds of Test 1 simulation.

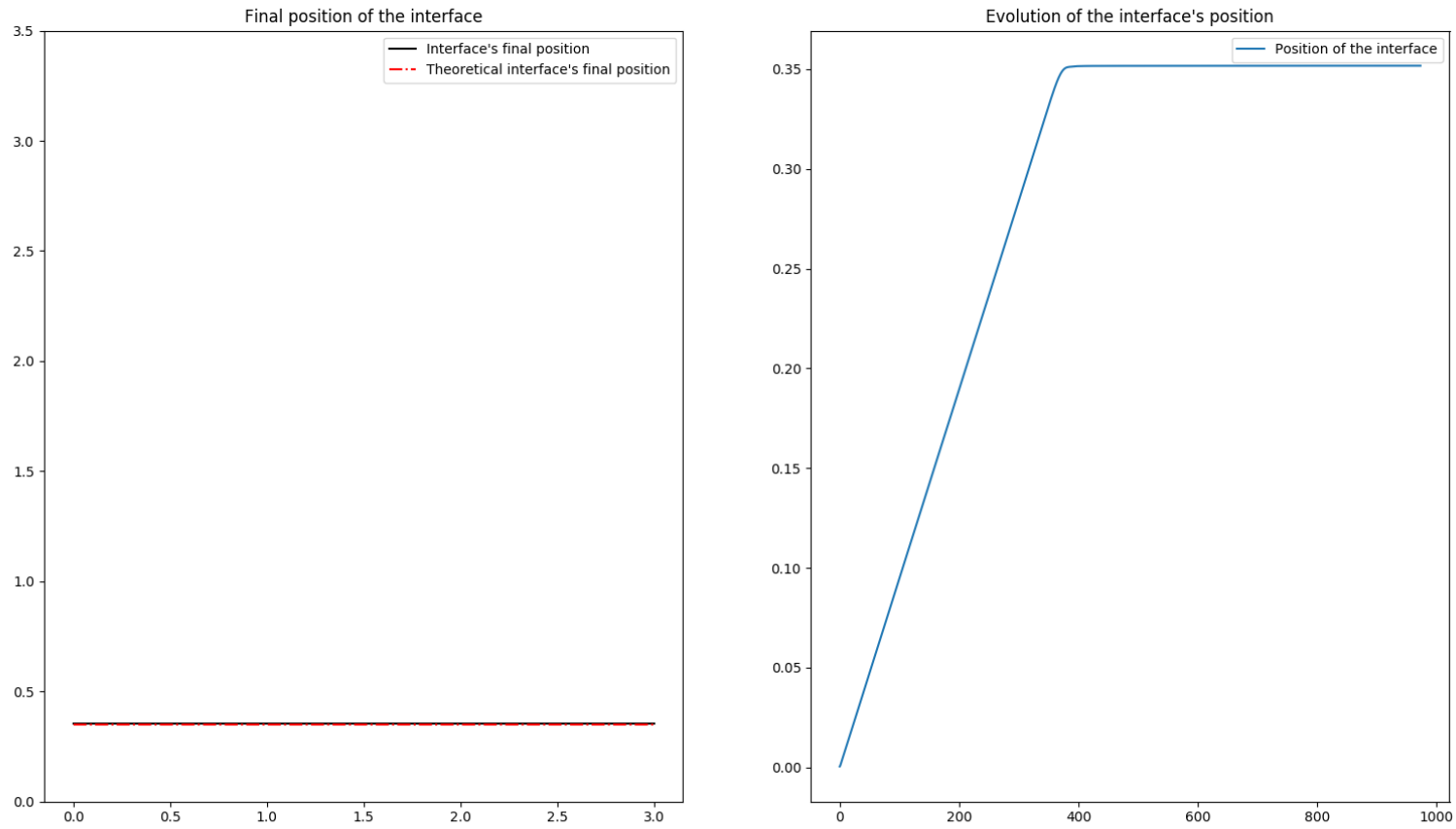


Figure 19: Evolution of free surface along Test 1 simulation.



Regarding the contour plots, the model works as expected. However, it can be noticed that there is some numerical diffusion as the transition from 0 concentration to 0.1 concentration is not perfectly sharp. This numerical diffusion is due to the interpolation scheme and can also be intuited from the evolution of fluid-sediment interface, which has some curvature rather than a sharp transition. This numerical effect can be controlled by using different interpolating strategies, however, its importance is relative as it is not affecting the sediment mass conservation.

From the final position of the sediment interface, it can be observed that it matches really well the expected position of 0.35 m from the reservoir bottom once all the sediment settles (including the small sediment volume which has been artificially transported by numerical diffusion). Although the monitoring of mass conservation presented some oscillations around a constant value, these were due to the integration method that was used to calculate the total mass, for this reason together with the fact that the final position of fluid-sediment interface was correct, it can be concluded that mass is properly conserved during the simulation.

4.2. Test case 2: sediment diffusion.

To analyze the sediment diffusion process, the previously tested advective transport is deactivated.

The case set-up is like the advective transport test, being the dimensions of the reservoir the same. However, in this case it is interesting to test how the sediment is eroded, how it passes to the fluid domain as sediment concentration and how is it distributed inside the fluid domain. For this reason, the initial position of fluid-sediment interface is 0.35 m from the bottom (equal to the final position in previous test). The eddy viscosity is raised to a fixed value of $10^{-5} \frac{m^2}{s}$, this is done to accelerate the diffusion process, as the relation between sediment transport and concentration gradient is driven by molecular and turbulent viscosity.

During the simulation, the total amount of sediment volume in the system is monitored by integrating the sediment volume inside each cell, this allows to detect mass conservation issues.

As there is no fluid motion inside the reservoir, the reference concentration is artificially set to 0.3, this means that the maximum value of the concentration inside the fluid domain cannot be higher than this value (as diffusive transport cannot generate local maximum values).

The results in this case are the contour plots of sediment concentration at each time step, they are presented in the following figure.

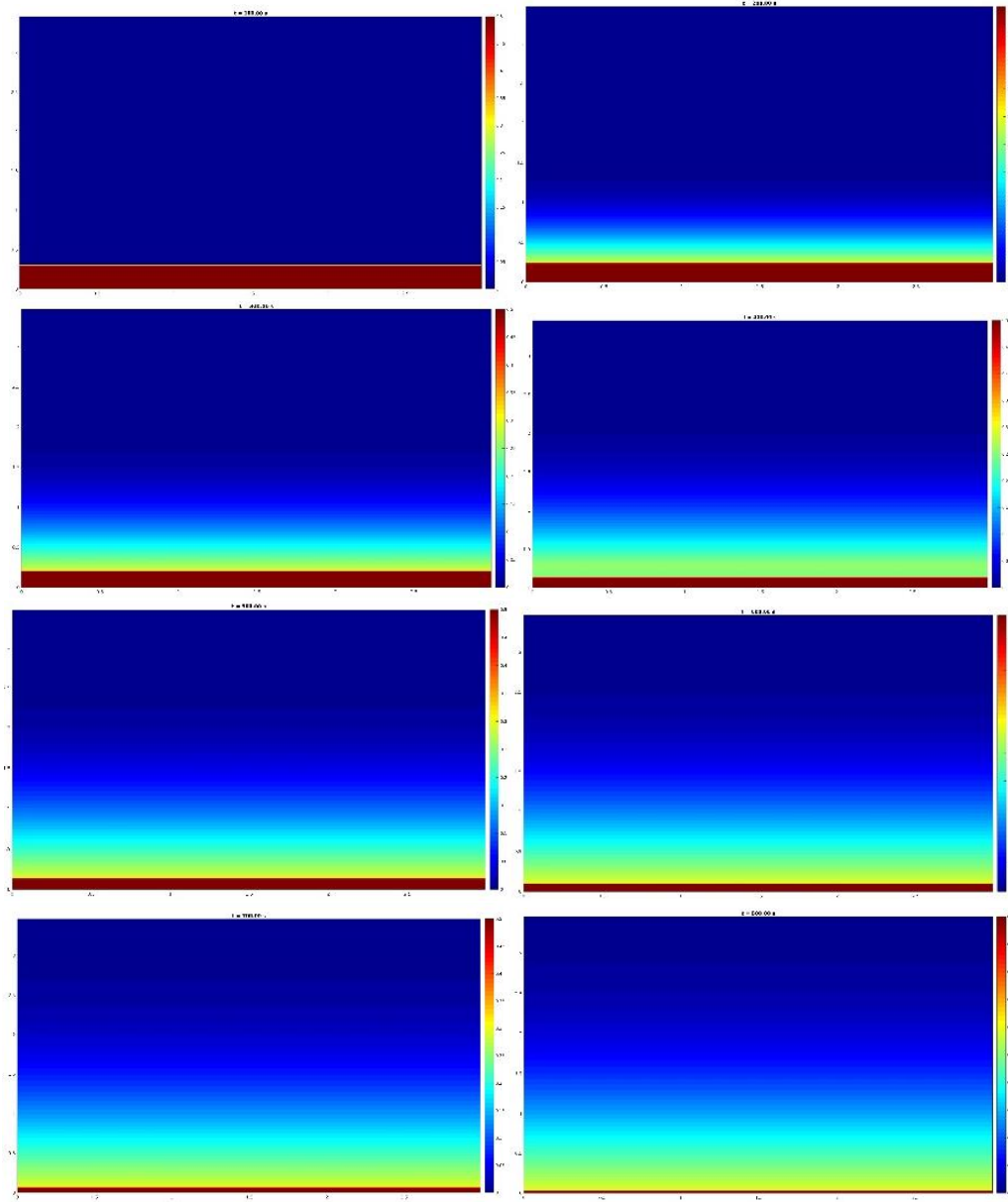


Figure 20: Contour plots of sediment concentration for Test 2.



During the test, no mass variations were detected apart from the previously described oscillations around a constant value.

The velocity at which the interface moves varies as the sediment concentration in the fluid increases during the simulation, this leads to a smaller concentration gradient and, consistently, a smaller sediment erosion.

Another important thing of this model is that it is not generating any maximum value inside the fluid domain, this is also true for the previous test case and is an important property for the transport of different properties inside the fluid.

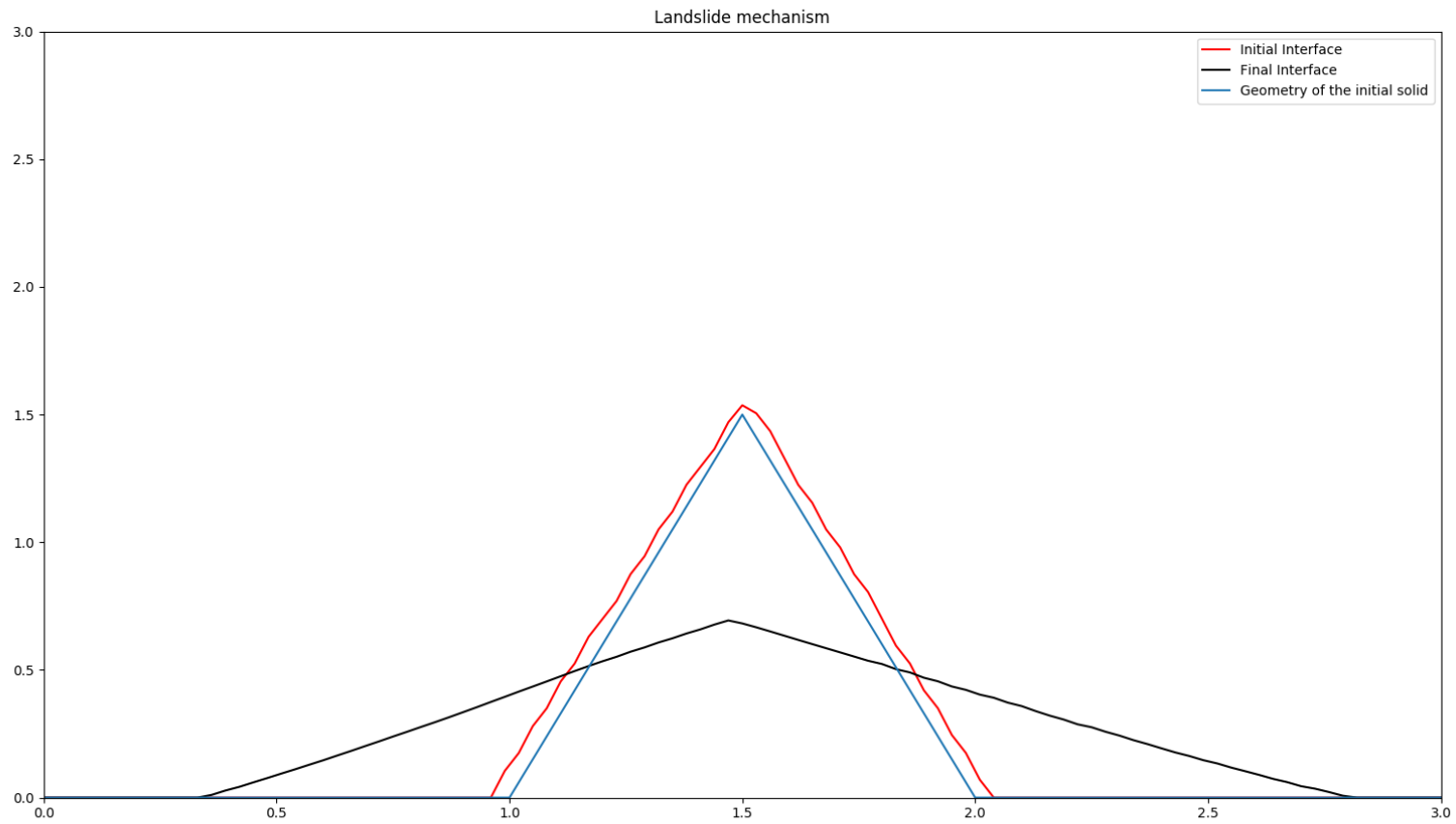
4.3. Test case 3: landslide mechanism.

When testing landslide mechanism, it is interesting to ensure that mass is conserved and that the slopes of resulting geometry are acceptable.

Recall that, for efficiency reasons, the landslide mechanism activates when the angle of repose is exceeded by, at least, 2° and finishes once the slope is at least 2° under the angle of repose.

The test setup consists in an initial geometry in triangle shape, the slope of the sides of this triangle is clearly larger than the angle of repose of the material, which is 33° . When the simulation starts, the numerical model is expected to generate a landslide in such a way that the final slope of the triangle is less than 31° .

As the landslide process is instantaneous, only the initial and final positions of fluid-sediment interface are obtained, however this information is enough to determine if landslides are done correctly. In addition, the geometry of the solid introduced in the meshing software (which is out of the scope of this work) is represented, as the interpolation done by this software affects the initial geometry of the model and, when considering the mass concentration, the geometry generated by the meshing software has to be taken into account.





As it can be seen from previous figure, the initial geometry introduced in the meshing software is not the same as the one in the final mesh, this problem can be solved by using a smaller cell size.

The initial the angle of slope (red line) is 45.6° while the resulting angle in the final geometry (black line in the figure) has a maximum slope of 30.8° . The initial geometry of the triangle is not perfectly symmetric, and neither is the resulting one.

Thus, it can be concluded that the landslide mechanism is behaving as expected.



5. Validation.

The validation process of this numerical model is still ongoing, as will be discussed in chapter 7. Once the initial test have been successful, the model is tested for more complex situations and compared with experimental results.

The hydrodynamic model has been already validated in different publications, thus, this part of the validation will be skipped in this work.

As a first step for this validation, the shear stress generated by the hydrodynamics on seabed is analyzed, this parameter has special importance as it drives completely the bedload transport. Furthermore, it controls indirectly (via shear stress) the sediment erosion

To test the shear stress generated by hydrodynamics, the model will be compared with data from (Sumer, et al., 2011), the experiment consisted in solitary waves breaking on a slope, shear stress was measured with load cells at different sections. The dataset provided by this publication consists in shear stress averaged over 40 solitary wave impacts and also the RMS.

In the following figures, a comparison between numerical model results (in blue line) and experimental results (black line for averaged value and red dashed line for RMS values) is presented. Sections have been named in the same way as in the publication, a schematic plot of the experimental set-up from the original publication is included.

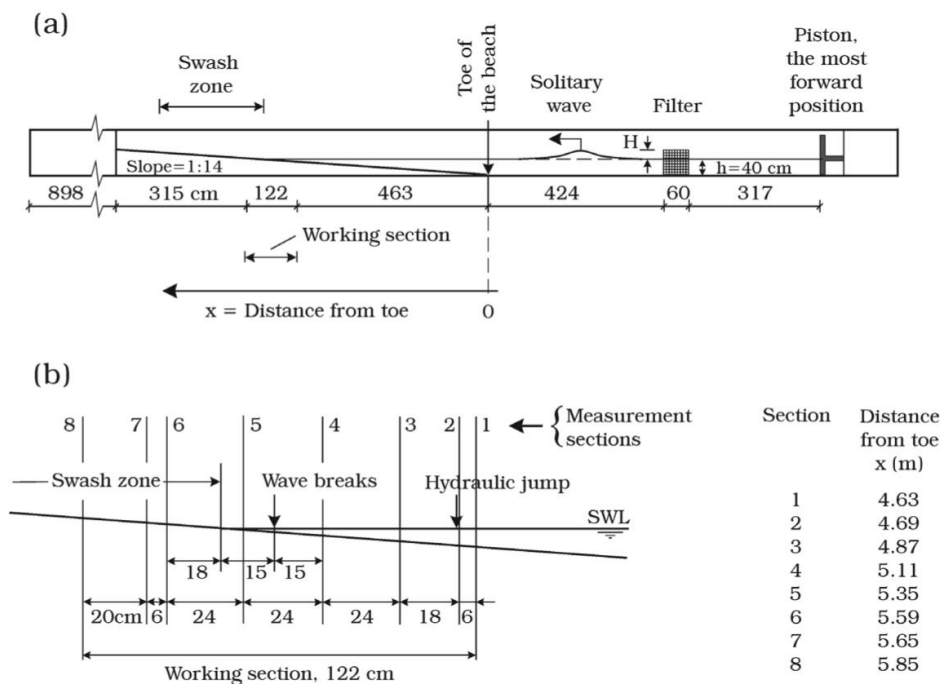
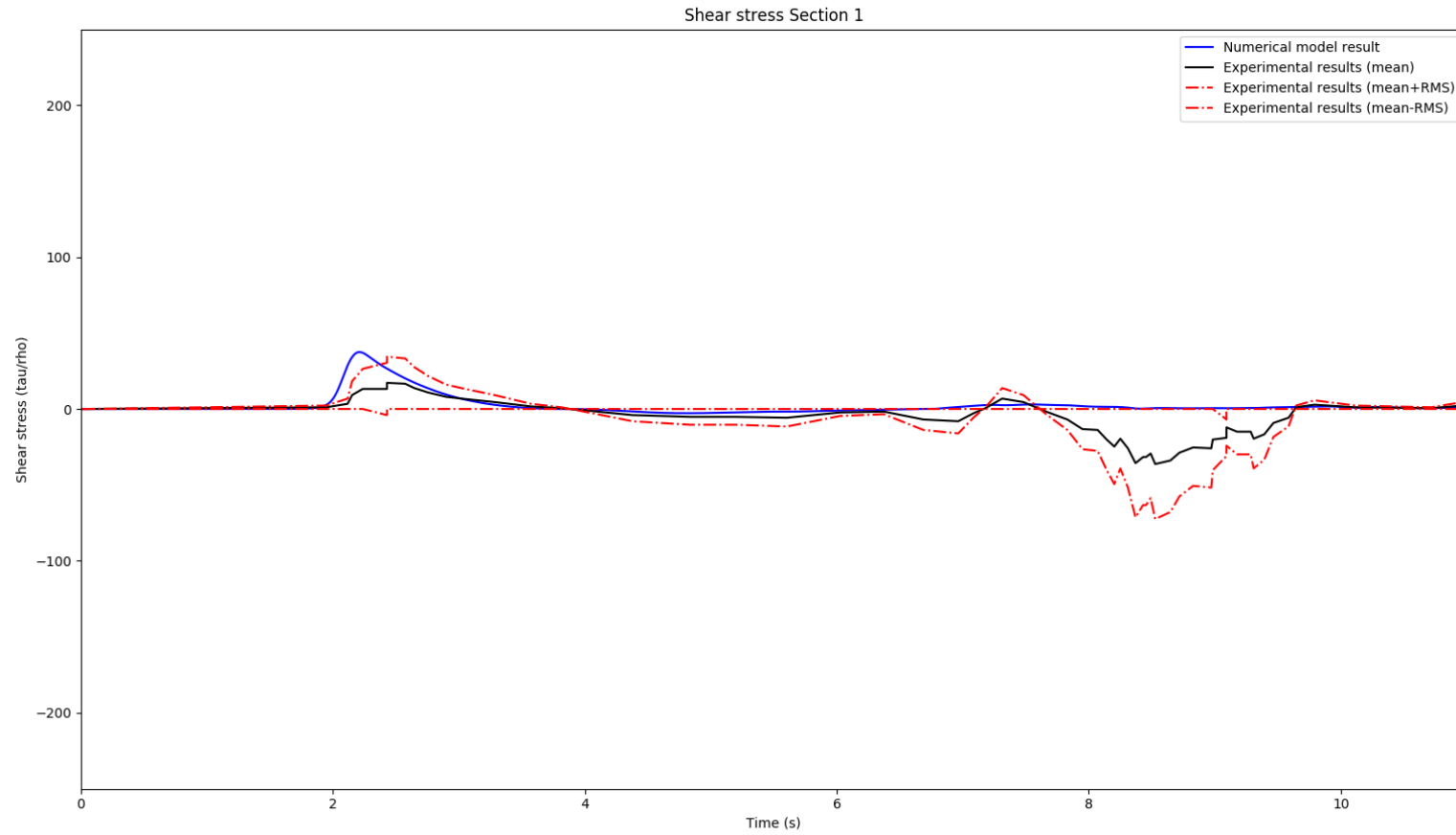
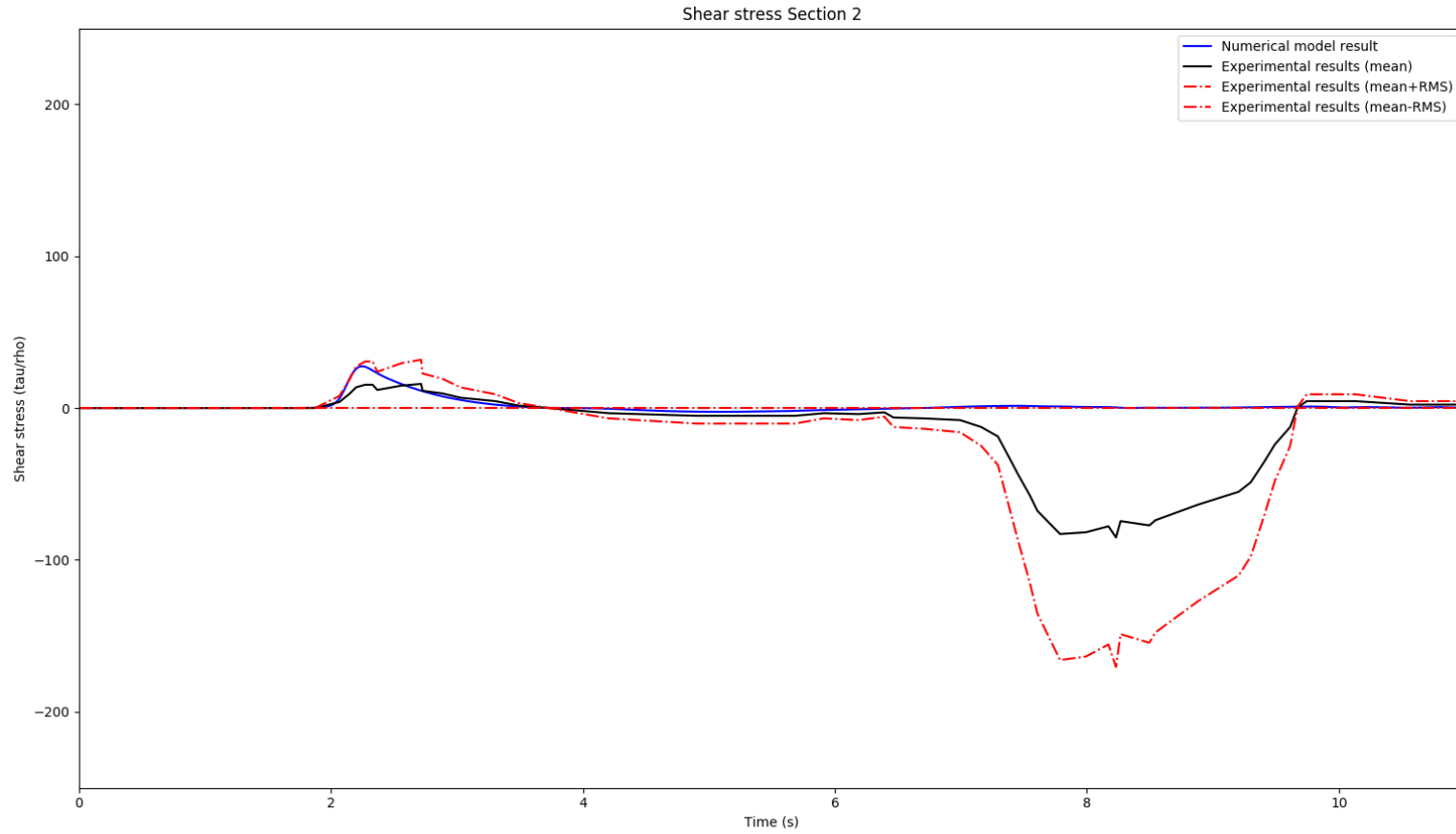
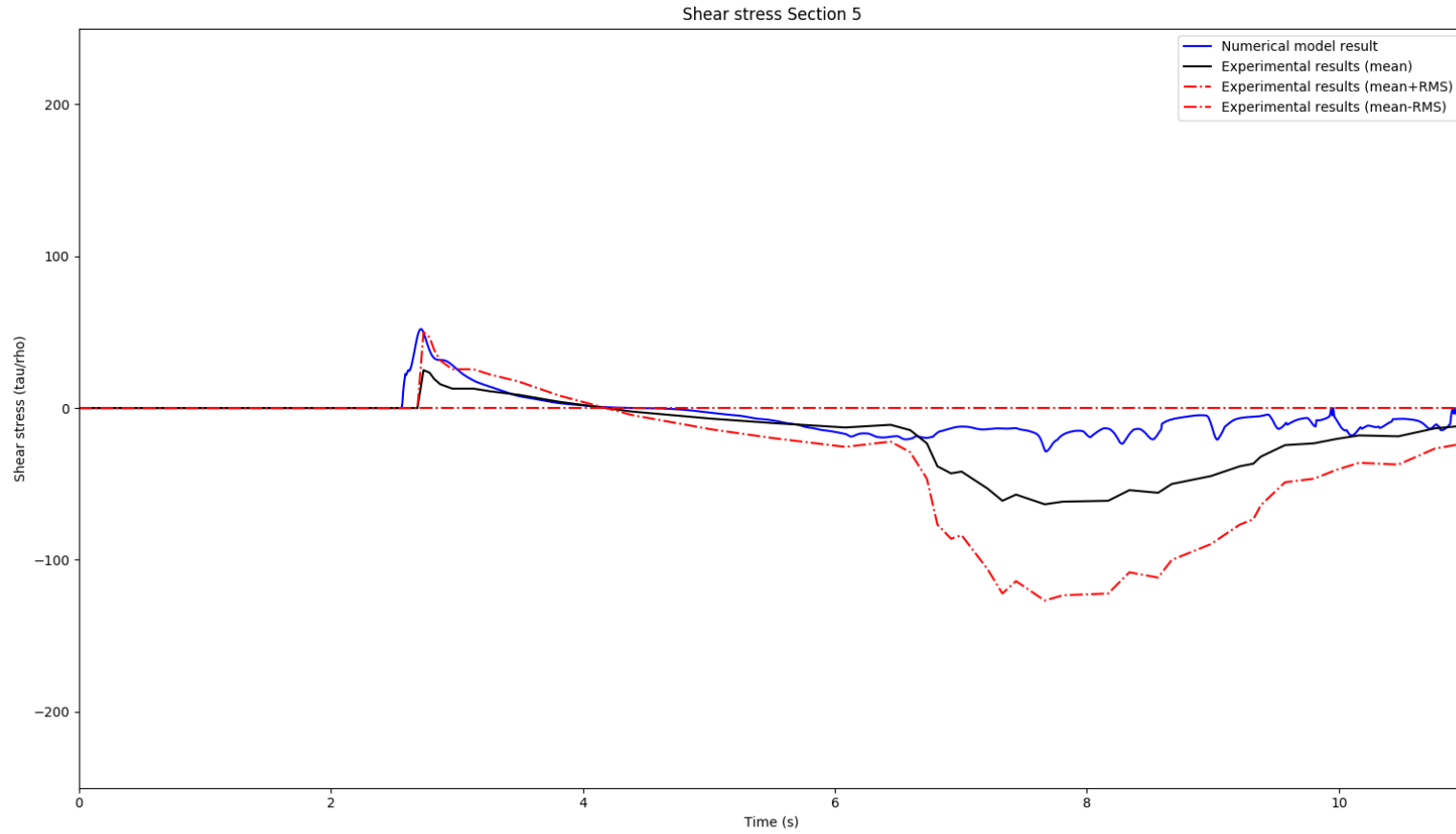
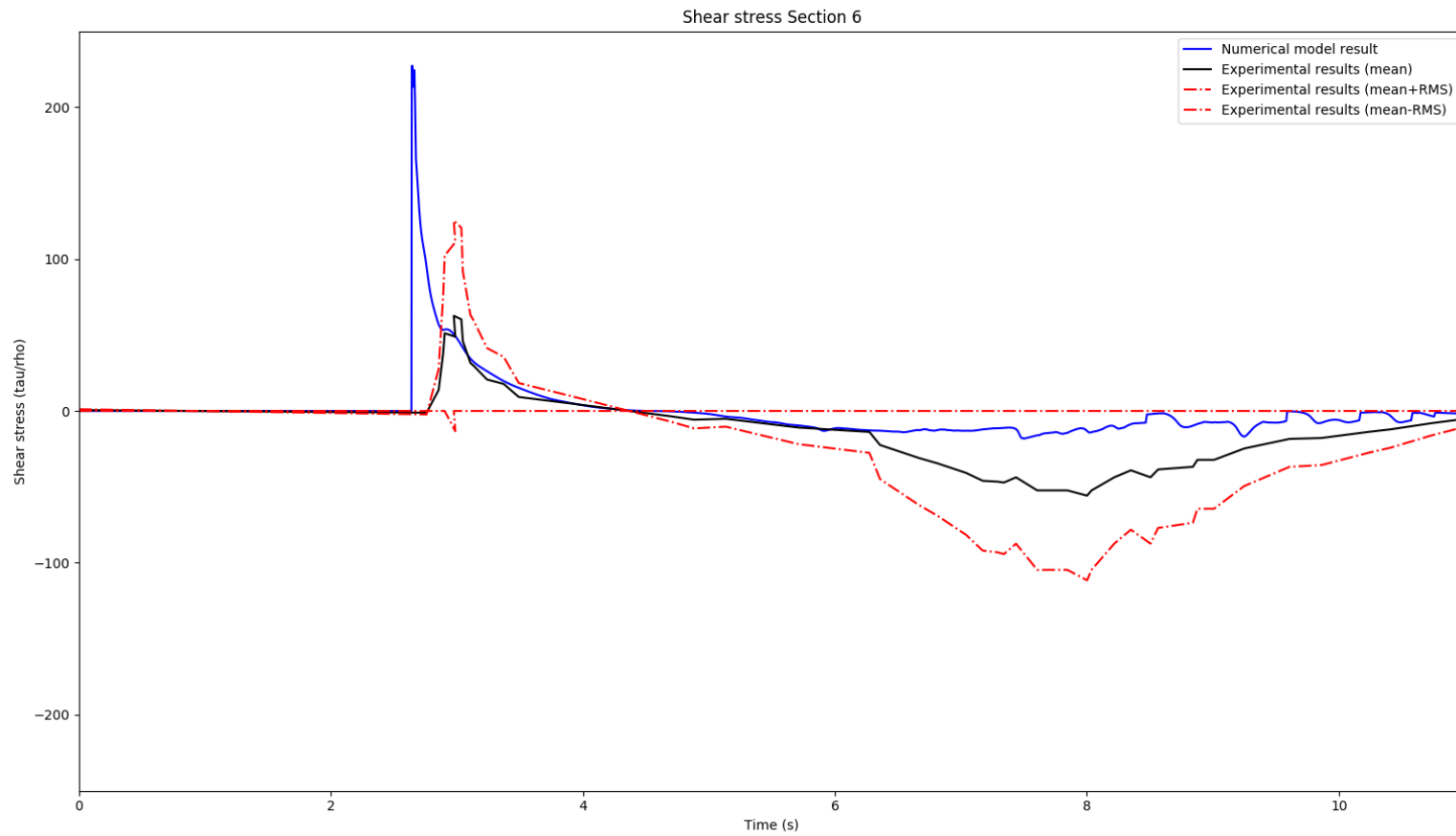


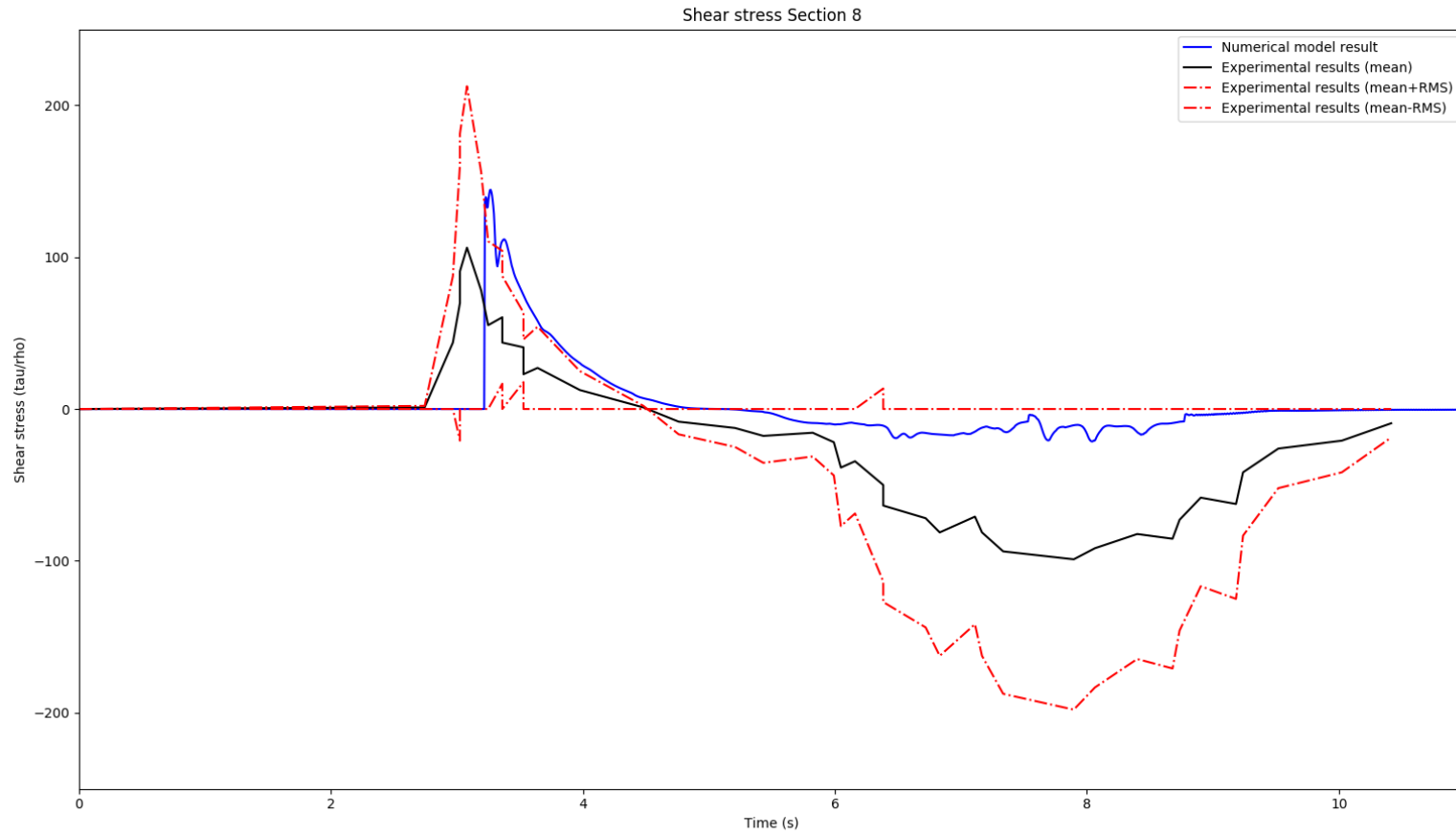
Figure 21: Experimental set-up of the experiments in validation case. Image taken from the original publication of the experiment (Sumer, et al., 2011)













From the previous results, there is a general agreement between numerical and experimental results, it is important to remark that data presented in the publication is an average of 40 waves while the numerical simulation has been done for only one case.

The most significant difference is on section S6 in which the numerical model predicts a larger value of shear stress than the experiments, the broken wave also passes 0.24 seconds earlier than the mean wave. Regarding that the RMS is of the same order of magnitude than the mean value, it can be concluded that this result is acceptable. Another aspect to take into account is that this section is particularly complex as it is in the swash zone and close to the breaking point of the wave.

Results for section 8 fit remarkably well to the experimental data even though section S8 is in the swash zone of the beach profile.

It can also be observed that the run-down is also well predicted by the numerical model, this is important aspect due to its importance for sediment transport in the beach profile.



6. Conclusions.

To conclude, this work generated a robust basis for a fluid-sediment interaction model. This model can transport suspended sediment, compute bedload transport, perform a sediment balance and move the fluid-sediment interface according to it.

In tests cases 1 and 2, the implementation of advective and diffusive transport has performed as expected as well as the complex boundary condition on fluid-sediment interface.

In test case 3, the landslide mechanism managed to produce a large variation in fluid-sediment interface satisfying the imposed physical restrictions for its slope and mass conservation.

In validation case, one of the most important parameter regarding the interaction between hydrodynamic and sediment transport models has been proved to work properly. This implies that the considerations in boundary layer characteristics fit this type of configurations.

Although some basic tests and validation have been done, there is some further work to do to achieve a fully functional model which can be used as a design tool for engineering projects, this will be discussed in the next section.

The modular implementation of the code is quite convenient in this sense, as it allows to develop new features and make changes in a faster way.



7. Further work.

The development of this numerical model requires some future work as commented before. On the other hand, it is interesting to test the ability of different kinds of models to solve more complex situations such as 3D configurations.

At the point of presenting this document, the numerical model is able to modify a beach profile generating a breaker bar, however, due to some problems with the implementation, it trends to generate sediment mass as the simulation advances. This can lead to large errors when simulations are long enough.

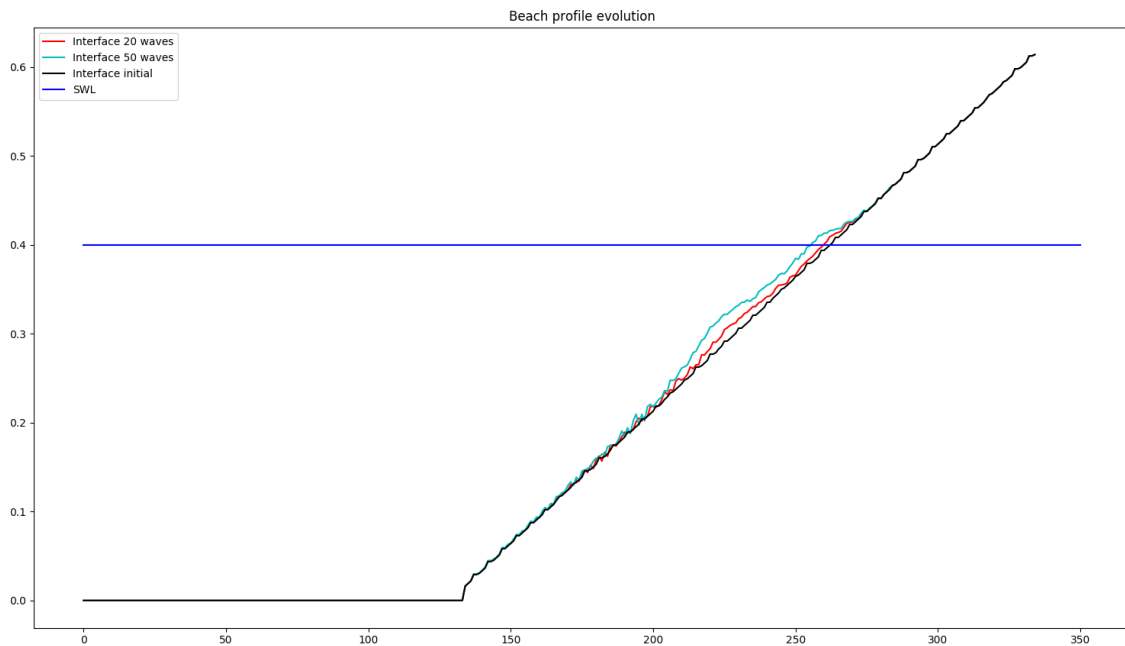


Figure 22: Beach profile predicted by the numerical model.

The suspended sediment transport is working properly from a qualitative point of view, although the previously commented problem can be related with it, this must be solved in order to fully validate the model. The following plots represent the concentration contours obtained with the model during a wave period, it can be seen how the wave puts sediment in suspension and transports it as it advances until it breaks.

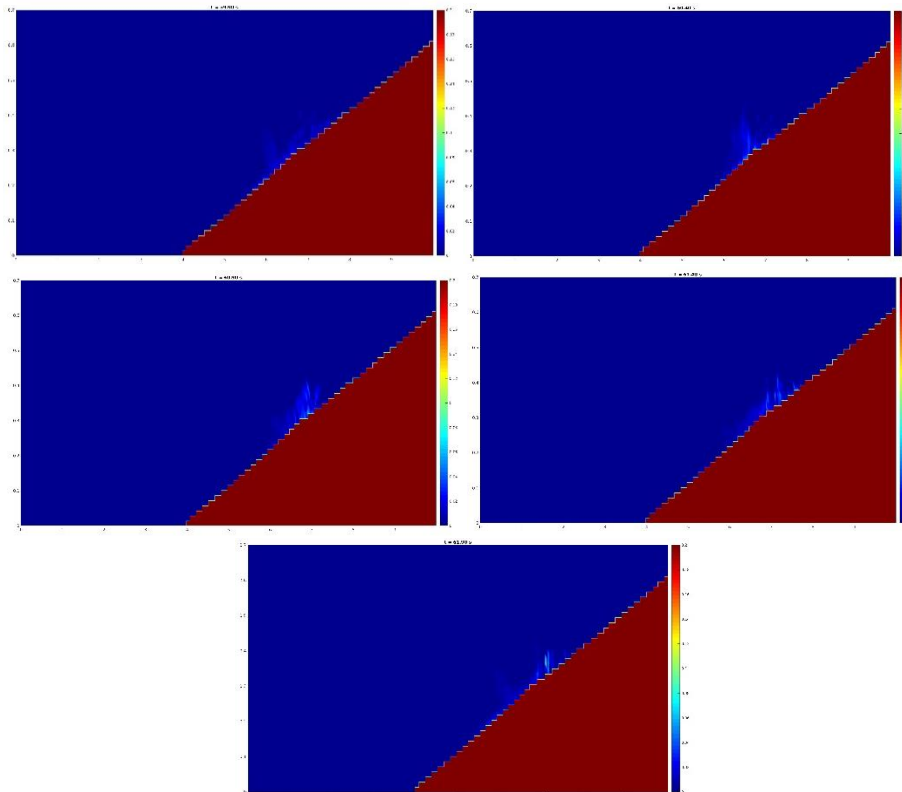


Figure 23: Contours of sediment concentration during a wave period.

Regarding the numerical model developed in this work, the scheduled future work can be summarized in the following points:

- As stated before, the validation of this model is still ongoing, and it is the most important part in future work. The ability of the model to develop a quantitatively correct beach profile under different wave conditions still has to be tested. This kind of problem involves both bedload and suspended sediment transport, as well as the complex hydrodynamics of wave breaking. It is planned to use data from (Baldock, et al., 2010) for this validation. Although at the moment of presenting this document the model is able to develop a beach profile under different wave conditions, some improvements have to be done in order to validate it for this purpose.
- Another interesting validation case is the scour in front of seawalls and rubble-mound breakwaters, the main challenge in these cases is to reproduce the hydrodynamics correctly with the recirculating cells at boundary layer scale.
- Some utilities also have to be developed such as automatic calculation of basic critical Shields parameter or different ways to input the angle of repose from different measured parameters of soil material (like static and dynamic friction coefficients). These utilities focus on improving the user experience.
- Regarding the various possible formulations for bedload sediment transport, reference concentration and others which have been used in the model, some decisions have to be taken to select the empirical formulae which better fits the configurations (type of sediment, hydrodynamics, etc.) where the model is intended to work. In this sense, it is important to keep developing the model following a modular structure which allows to change these features fast.



- In the implementation, some extra work has to be done to improve the numerical methods used for different tasks. For example, at the moment when this work is presented, different implementations of smoothing algorithms for bedload transport are being tested to improve the efficiency and stability of the model.

On the other hand, there is some planned future work with other types of numerical models for sediment transport commented in chapter 2, in particular, Lagrangian two-phase models offer promising possibilities to address complex physics such as landslide induced tsunamis or analysis of construction processes in different climatic conditions.



References.

- Baldock, T., Manoonvoravong, P. & Pham, K. S., 2010. Sediment transport and beach morphodynamics induced by free long waves, bound long waves and wave groups.. *Coastal Engineering*.
- Boyer, F., Guazzelli, É. & Pouliquen, O., 2011. Unifying Suspension and Granular Rheology. *Physical Review Letters*.
- Chauchat, J. y otros, 2017. SedFoam-2.0: a 3-D two-phase flow numerical model for sediment transport. *Geoscientific Model Development*.
- Einstein, A., 1906. Eine Neue Bestimmung der Molekuldimensionen. *Annals of Physics*.
- Engelund, F. & Fredsoe, J., 1976. A Sediment Transport Model for Straight Alluvial Channels. *Nordic Hydrology*.
- Fredsoe, J. & Deigaard, R., 1992. *Mechanics of Coastal Sediment Transport*. Singapore: World Scientific Publishing.
- Jacobsen, N. G. & Fredsoe, J., 2014. Formation and development of a breaker bar under regular waves. Part 2: Sediment transport and morphology.. *Coastal Engineering*.
- Jacobsen, N. G., Fredsoe, J. & Jensen, J. H., 2014. Formation and development of a breaker bar under regular waves. Part 1: Model description and hydrodynamics. *Coastal Engineering*.
- Jasak, H. & Tukovic, Z., 2006. Automatic Mesh Motion for the Unstructured Finite Volume Method. *trans. FAMENA*.
- Krieger, I. M. & Dougherty, T. J., 1959. Mechanism for Non-Newtonian Flow in Suspensions of Rigid Spheres. *Journal of Rheology*.
- Kundu, P. K., Cohen, I. M. & Dowling, D. R., 2012. *Fluid Mechanics*. 5th Edition ed. s.l.:Elsevier.
- Lin, P., 1998. *Numerical Modelling of Brekaing Waves*. s.l.:Cornell University.
- Luque, R. F., 1974. *Erosion and transport of bed sediment. Dissertation*. s.l.:Jrips Repro.
- Papadopoulos, D., 2013. *Scour below the toe of breakwaters*. s.l.:TU Delft, department of hydraulic engineering..
- Peng, Z., Zou, Q.-P. & Pengzhi, L., 2018. A partial cell technique for modeling the morphological change and scour.. *Coastal Engineering*.
- Roulund, A., Sumer, B. M., Fredsoe, J. & Michelsen, J., 2005. Numerical and experimental investigation of flow and scour around a circular pile.. *Cambridge University Press*.
- Sumer, B. M. y otros, 2011. Flow and sediment transport induced by a plunging solitary wave.. *Journal of Geophysical Research*.
- Tukovic, Z. & Jasak, H., 2012. A moving mesh finite volume interface tracking method for surface tension dominated interfacial fluid flow.. *Computers and Fluids*.
- van Driest, E. R., 1956. On turbulent flow near a wall. *J. Aeronaut. Sci.*